國 立 交 通 大 學

電信工程學系

碩 士 論 文

應用於語音之三階三角積分數位類比轉換器

A 3rd-order Delta-Sigma Digital to Analog Converter for Audio Application

研究生：黃 介 仁

指導教授：洪 崇 智 教授

應用於語音之三階三角積分數位

類比轉換器

A 3$^{\text{rd}}$-order Delta-Sigma Digital to Analog Converter for

Audio Application

研 究 生：黃介仁　　　　　　Student：Chieh-Jen Huang

指導教授：洪崇智 教授　　　　Advisor：Prof. Chung-Chih Hung

國 立 交 通 大 學

電 信 工 程 學 系 碩 士 班

碩 士 論 文

A Thesis

Submitted to Department of Communication Engineering

College of Electrical and Computer Engineering

National Chiao Tung University

in Partial Fulfillment of the Requirements

for the Degree of

Master of Science

in

Communication Engineering

Septemper 2008

Hsinchu, Taiwan.

中 華 民 國 九 十 七 年 九 月

應用於語音之三階三角積分數位

類比轉換器

研究生：黃介仁　　　　　　　　　　　指導教授：洪崇智 教授

國立交通大學

電信工程學系碩士班

摘要

近年來因為語音產品的蓬勃發展，如 MP3 隨聲聽等等，使得語音系統數位類比轉換器成為一個重要的目標。而對於用電池運作的語音系統有幾個問題是我們必須注意的。因為功率消耗會影響電池的壽命，所以必須把功率消耗設計的越小越好。另外，為了達到多媒體產品的品質需求，此數位類比轉換器必須達到約 16 位元的高解析度。

三角積分數位類比轉換器(Delta-Sigma D/A converter)是一種廣泛運用的技術，它能夠達到高解析度、降低數位電路部份的操作速度、能夠緩和頻帶外(out-of-band)濾波器的需求以及提高對時脈抖動(clock jitter)的免疫力。使用直接電荷轉換的切換式電阻電容技術可以減少 KT/C 雜訊和元件不匹配的影響而不增加功率消耗，並且比直接電荷轉換切換式電容技術擁有較少的失真。資料加權平均的演算法可以抑制電容之間的不匹配所造成的非線性度。

在此研究中我們將介紹一個 15 等級量化、三階的三角積分數位類比轉換器，取樣頻率是 44.1 千赫茲，輸入訊號為 24 位元，因為超取樣倍率為 64 倍，所以主要時脈操作在 2.8224 百萬赫茲，本次設計的晶片是由晶片中心(CIC)提供的台積電(tsmc)標準 0.18 微米製程中實現。在 1.8 伏特的供應電壓下可達 87 分貝的動態範圍，並且消耗 8.25 毫瓦特。

A 3rd-order Delta-Sigma Digital to Analog Converter for Audio Application

Student：Chieh-Jen Huang   Advisor：Prof. Chung-Chih Hung

Department of Communication Engineering

National Chiao Tung University

Hsinchu, Taiwan

Abstract

Audio digital-to-analog converters (DAC) have played an important role recently with the rapid growth of the cellular phone and portable audio devices. There are some main issues for a battery-operated audio system. Power dissipation affects the battery life, so it must be as low as possible. A high resolution of about 16bits is required for the DAC to meet the quality of the media.

The delta-sigma D/A converters have been used extensively. It can achieve high resolution, reduce digital circuit speed, relax the requirements of the out-of-band filter, and enhance immunity to clock jitter. Using the direct charge transfer switched-RC (DCT-SRC) technique in the multi-bit reconstruction DAC can reduce kT/C noise and element mismatch without increasing power dissipation. And this kind of DCT-SRC DAC has smaller distortion than direct charge transfer switch capacitor DAC (DCT-SCDAC). The data weighted averaging algorithm restrains nonlinearity caused by the mismatch of capacitors.

A 15-level quantization, third-order delta-sigma DAC is presented. Its sampling rate is 44.1 kHz with 24-bit input. The main clock is 2.8224 MHz because of the 64X oversampling ratio. This DAC implemented in a TSMC 0.18um CMOS process achieved 87dB dynamic range (DR), while consuming 8.25mW from a 1.8V supply.

誌謝

首先感謝我的指導教授洪崇智老師，在我兩年的研究生活中提供良好的學習環境，以及這段日子來對我的指導與照顧，並且在研究主題上給予我寬廣的發展空間。同時我也要感謝在這碩士班兩年內曾經教過我的每位老師，由於他們熱心的教學，使我在短短的碩士班兩年內，學習如何設計並且製作數位、類比積體電路。還有要感謝國家晶片系統設計中心提供先進的半導體製程，讓我有機會將所設計的電路得以實現並完成驗證。

其次，我要感謝羅天佑學長、楊家泰學長、蔡宗諺學長、白逸維學長、廖德文學長、邱建豪學長和高正昇學長在研究上的指導與幫助，透過和學長之間的討論，使我的基礎觀念更加清楚紮實，並且教導我如何使用各種儀器，以及協助解決量測時所遇到的問題。接著還要感謝夏竹緯、楊文霖、林永洲、郭智龍、邱楓翔和張維欣等諸位同窗，與我在實驗室一同奮鬥，還有李尚勳、黃聖文、許新傑和簡兆良等學弟的支持。

特別要感謝我的父母和家人，感謝他們提供了一個穩定且健全的環境，使我無後顧之憂地完成我的學業。最後要感謝我的女朋友，感謝她一直默默的支持我、鼓勵我，並在這段成長的路上與我相伴。

總而言之，我要感謝所有關心我、愛護我和曾經幫助過我的人，願我在未來能有一絲的成就獻給最愛我的家人、老師以及朋友，謝謝你們。

黃介仁

國立交通大學
中華民國九十七年九月

Table of Contents

List of Figures

Chapter 5

List of Tables

Chapter 1

Introduction

1.1 Motivation

The growth for portable devices used in applications such as mobile computing, consumer electronics, etc. has increased the demand for an low power high performance audio digital-to-analog converter (DAC). Power dissipation directly effects battery life, so it must be as low as possible. In, addition, using fully differential or single-ended input/output signals affects the pin count. After considerations of overall factors, the requirements for audio DAC should meet features of low power consumption [1], dynamic range above 16-bit (i.e., 96dB). A delta-sigma(Δ-Σ) data converter is popular by its inherent high resolution and low power characteristics. Switched-capacitor circuits provide a robust technique for building analog signal processing blocks in CMOS process. The inherent charge storing ability of CMOS technology enables accurate signal processing in mixed-signal applications such as filters and data converters using switched-capacitor circuits.

In this research, a low power and high resolution audio delta-sigma digital-to-analog converter has been designed with the digital and analog circuit implemented with the standard TSMC 0.18μm CMOS 1P6M process. The parts of interpolator, delta-sigma modulator and switched capacitor filter are emphasized. The decrease in oversampling ratio can decrease the digital circuit speed and then we can achieve the goal of power consumption decrement. A high SNR (signal-to-noise ratio)

1

is performed in the delta-sigma modulator because of noise shaping function. However, the dynamic range and SNDR (signal-to-noise plus distortion ratio) are decided by noise and distortion caused by the analog circuit. In order to reduce total harmonic distortion, a circuit combined direct-charge-transfer technique and Switched-RC technique is used.

1.2 Thesis Organization

The six chapters of this thesis are organized in the following structure:

In Chapter 1, the thesis is briefly introduced.

In Chapter 2 fundamentals of the delta-sigma audio DACs are described. Nyquist sampling and oversampling are compared. Noise shaping technique is reviewed. One-bit and the multibit quantizers are compared. The unit-element DAC and nonlinearity, introduced by its mismatch errors, are described. A general audio DAC structure and the function of each block are discussed.

In Chapter 3, design of a digital interpolation filter and noise shaper are covered. An interpolator with a 64 interpolation factor and a third-order, fifteen-level delta sigma noise shaping loop are included. A thermometer encoder and a data weighted averaging encoder are discussed.

In Chapter 4 introduces the conventional SCDAC, DCT-SCDAC and the DACs that are proposed recently. Some Class-AB amplifier are discussed. Finally, designed 1.8V delta-sigma audio DAC is described.

Finally, the conclusions of this thesis are summarized in Chapter 5.
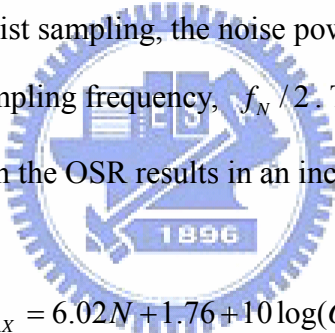
Chapter 2

Delta Sigma Digital-to-Analog Converters

2.1 Oversampling

Oversampling technique is widely used to achieve high resolution in data converters. It is using a higher sampling rate than the Nyquist rate. The factor oversampling ratio (OSR) is defined as $OSR = f_s / 2f_B$. Figure 2.1(a) and (b) are output spectra of a Nyquist sampling, the noise power spreads over signal band, f_B, which is half the sampling frequency, $f_N / 2$. The last term of Eq 2-1 shows that an double increase in the OSR results in an increase in SNR by 3dB.

$$SNR_{MAX} = 6.02N + 1.76 + 10\log(OSR) \quad (\text{dB}) . \qquad (2\text{-}1)$$

2.2 Noise shaping

Though oversampling is a very simple way to improve SNR, it is not very practical to obtain very high resolution such as 16-20bits. In delta-sigma modulation (DSM), noise shaping is employed to relax OSR or, in other words, obtain higher SNR. The noise shaping property of the delta-sigma modulator can suppress the in-band quantization noise as depicted in Fig 2.1 (c).
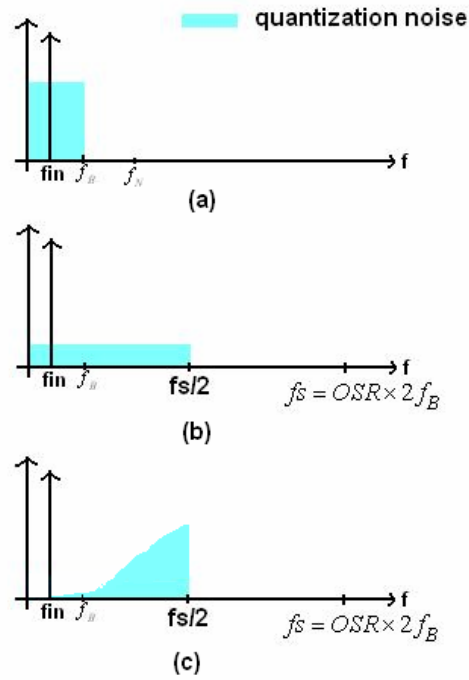
Figure 2.1 Spectra of (a) a Nyquist sampling (b) an oversampling, and (c) an

oversampling with noise shaping
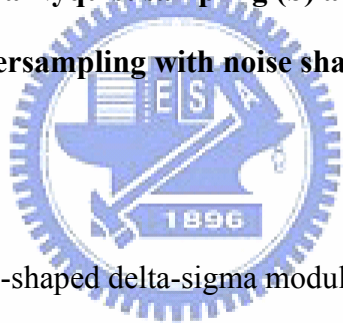
A linear model of a noise-shaped delta-sigma modulator is shown in Figure 2.2.
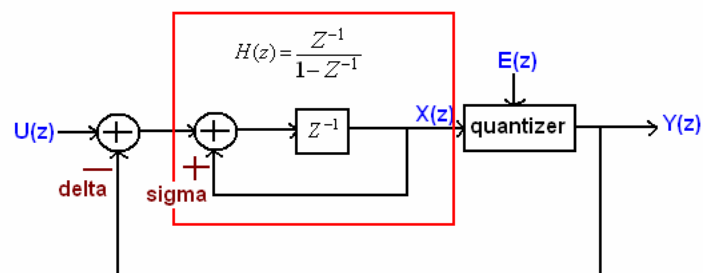
Figure 2.2 Linear model of the modulator

The ouput in z-domain can be expressed as:

$$Y(z) = STF(z)U(z) + NTF(z)E(z) \qquad . \qquad (2\text{-}2)$$

where

$$STF(z) = \frac{H(z)}{1 + H(z)} \quad . \tag{2-3}$$

$$NTF(z) = \frac{1}{1 + H(z)} \tag{2-4}$$

The STF(z) is the input signal transfer function and NTF(z) is the noise transfer function. The quantization noise is indicated by E(z). The loop filter transfer function, H(z) of the first-order DSM must be a highpass function. Beacause the zeros of NTF(z) are equal the poles of H(z), we can get $H(z) = \frac{Z^{-1}}{1 - Z^{-1}}$. Therefore, The Eq 2-2 can be rewritten as :

$$Y(z) = z^{-1}U(z) + (1 - z^{-1})E(z) \tag{2-5}$$

The quantization noise is shaped by a first-order differentiator. The quantization is shaped by a first-order differentiator. That results in reduced noise power in the signal band, f_B, and increased noise power out of the signal band. Figure 2.3 shows the general shape of zero-order, first-order, and second-order noise-shaping curves. The noise power over the band of interest decreases as the noise-shaping order increases. However, there are some issues about increase of out-of-band noise and stability for the higher-order modulators.
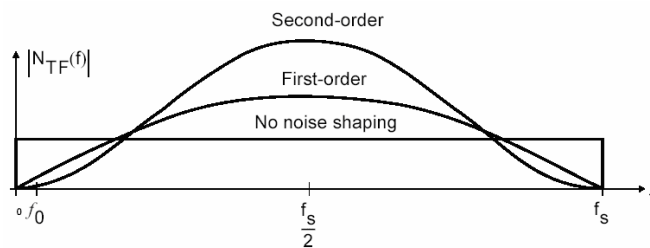
Figure 2.3 Different orders of the noise-shaping transfer functions

6

2.3 Comparison of One-bit and Multi-bit implementations

The comparison of one-bit and multibit modulators is based on oversampling ratio, linearity, stability, and out-of-band quantization noise. The main advantage of one-bit modulator is inherently linear since it only need to produce two output levels and two points can define a straight line. However, the one-bit modulator with higher-order is easy to become unstable. A stable modulator is defined as one in which the input to the quantizer remains bounded and the quantization does not become overloaded. An overloaded quantizer means its input signal is over the quantizer's normal range. It causes the quantization error to be greater than $\pm\Delta/2$. Another disadvantage of one-bit modulator is to result in a large amount of out-of-band quantization noise, which must be significantly reduced by the analog circuit. Such a task requires relatively high-order analog filtering. It increases the difficulty in designing the analog filtering circuit.
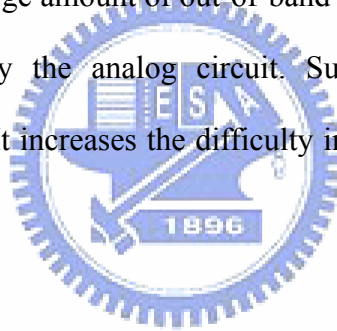
A multibit modulator can provide the improvement in SNR. From the first term of formula (2-1), SNR increases 6 dB with increasing one bit in the quantizer output. Therefore, a multibit modulator of a given order can achieve the target of dynamic range with less oversampling ratio than a one-bit modulator of the same order. In the application of higher-order modulators, a multibit modulator is also more stable than a one-bit modulator [2]. Additionally, the use of the multibit modulator can significantly reduce the large amount of out-of-band quantization noise and tolerate relaxed out-of-band filter specifications, but it must take care to ensure the multibit output of the modulator remains linear. The linearity of the multi-level output is limited by the mismatches in the components which are used to generate the analog levels. The diagram of step mismatches in the D/A converter is shown in Figure 2.4.
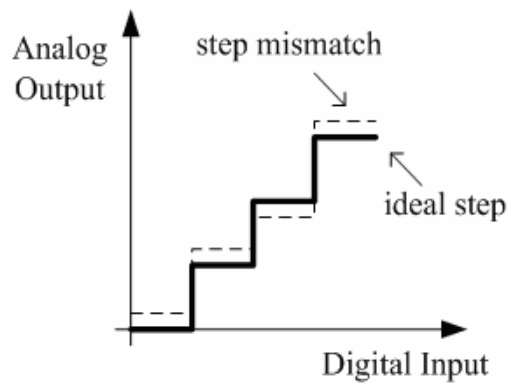
Figure 2.4 Illustration of step mismatch in the D/A converter

These step mismatches caused by component mismatches result in the distortion over the signal band, and then reduce the obtained SNDR (signal-to-noise plus distortion ratio). In order to solve the mismatch problem, various linearization techniques have been proposed, such as trimming and dynamic element matching (DEM). The trimming technique is practical for a D/A converter to enhance the matching property of identical components. It does not require extra circuits to reduce mismatch effect if each component is trimmed individually. However, trimming technique is expensive, time-consuming, and not a one-time process since device aging and temperature variation occurring in the lifetime of a D/A converter reduce the effect of compensating mismatches. The algorithm of DEM will be discussed in the following section.

2.4 Oversampling delta-sigma DACs

Delta-sigma data converters employ noise shaping and oversampling to achieve a wide dynamic range in the band-of-interest. It is extremely suitable for the audio application. Figure 2.5 shows its block diagram. The input signal is an N-bit sampled data with sampling frequency fs, which is often slightly larger than Nyquist rate. By passing through an interpolation filter(IF), its sampling frequency is increased to Lfs, and the images introduced by oversampling are removed. The output of the interpolation filter then feeds into the noise-shaping loop (NL) to M-bit output (M is much smaller than N). These truncated bits then converted to the analog signal by an internal M-bit DAC. The quantization noise brought by the noise shaping process (most of the noise power is out of the interested signal band) is filtered by the following lowpass filter and the smoothed analog signal output results.
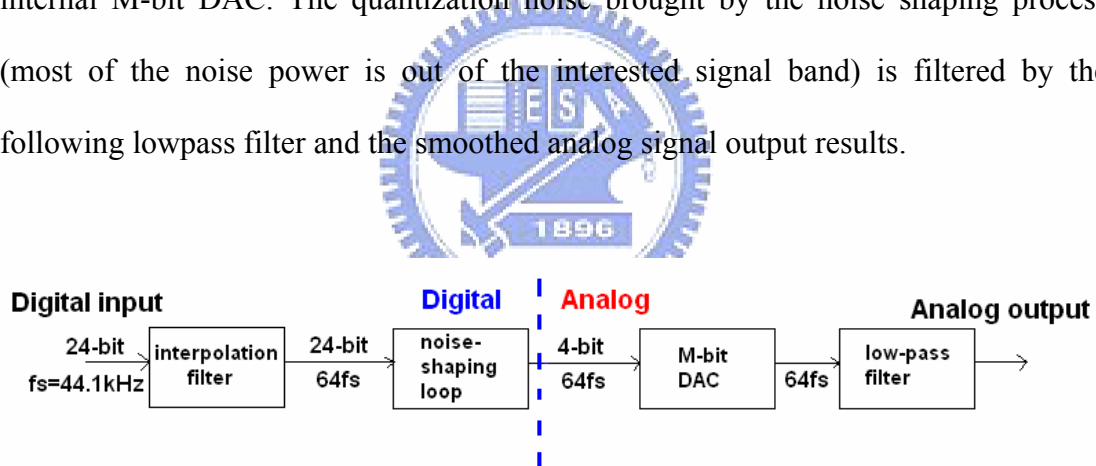
Figure 2.5 Block diagram of a delta-sigma DAC.

The sources of error in the delta-sigma DAC are the device mismatch which causes harmonic distortion, rather than component noise, device nonlinearities, clock jitter sensitivity and inband quantization error from the delta-sigma modulator.

The signals spectra for each stage are illustrated in Figure 2.6.
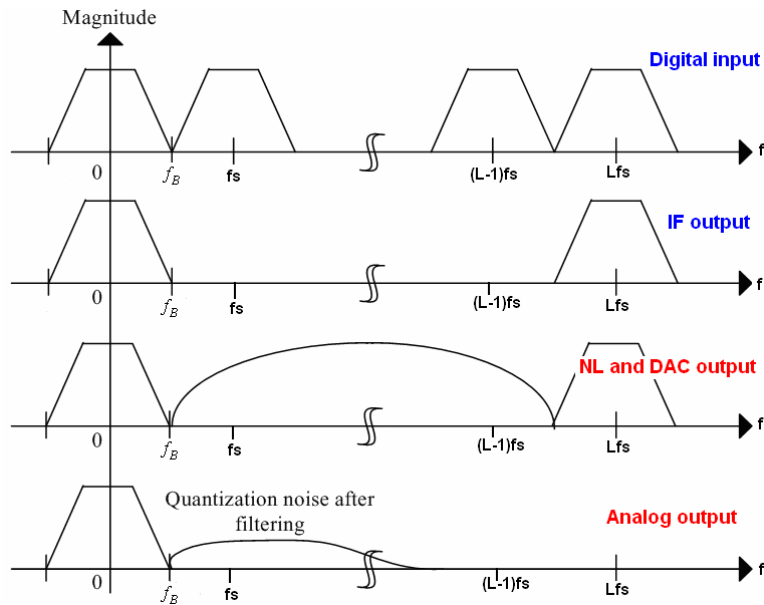
Figure 2.6 Frequency spectra at different points of the delta-sigma DAC

A widely used structure for the M-bit internal DAC in the delta-sigma DAC is a so called unit-element DAC which is built from unit elements such as capacitors in a switched-capacitor circuit or current sources in a current-steering DAC. An advantage of such a DAC is that there are no glitches at its output [3]. Figure 2.7 shows the diagram of the unit-element DAC.
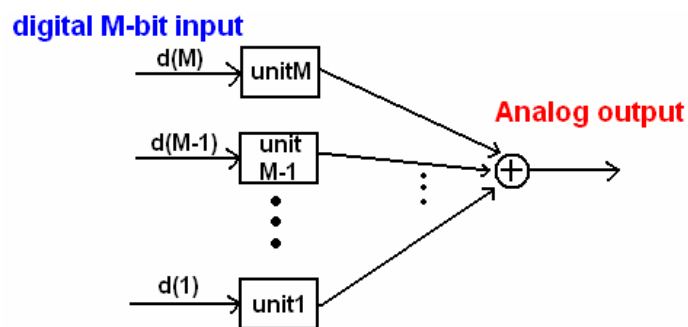
Figure 2.7 the unit-element of DAC

Chapter 3

Implementation of the Digital circuits in ΔΣ DAC design

3.1 Interpolation filter design

3.1.1 1bit to 24bit converter

In order to save the chip's pin count, the 1bit serial input data is converted into 24bit parallel output data for the signal processing performed in interpolation filter.

3.1.2 Principle of interpolation filter design
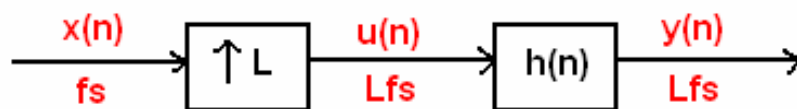
Figure 3.1 Block diagram of interpolation filter

The interpolation filter used in the delta sigma DAC is built by an upsampler and a lowpass filter as shown in Figure 3.1. The digital input signal x(n) is upsampled to u(n) by an oversampling ratio L. If the sampling rate of x(n) is a Nyquist rate f_s, the sampling rate of u(n) will be $L\ f_s$. The Figure 3.2 shows the detail about how to increase sampling rate.
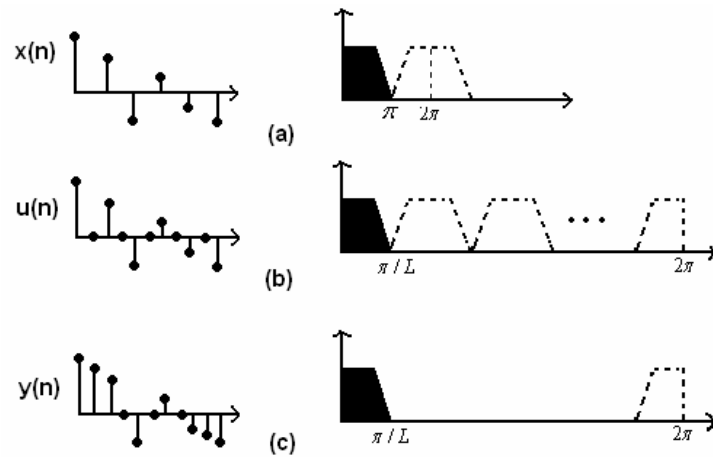
Figure 3.2 Interpolator's spectrum

For example of oversampling ratio L , the input signal x(n) is converted into u(n) by inserting L-1 zero-valued samples between two consecutive samples of the input sequence x(n). The graph of Figure 3.2(a)(b) show the difference between x(n) and u(n). A low-pass filter h(n) is necessary to filter out the undesired image signal shown in the graph of Figure 3.2(c).

The anti-image filter is used to remove undesired images signal which replace the inserted zero value samples with proper values in time domain. The strict requirements on the linear phase characteristics in audio applications mandate the use of a finite impulse response (FIR) filter, rather than an infinite impulse response (IIR) filter. However, high order is necessary for a sharp cutoff FIR filter. Equation 3-1 gives the transfer function of typical FIR filter.

$$H(z) = \sum_{n=0}^{N-1} h(n)z^{-n}, \qquad h(n) \text{ real.} \qquad (3\text{-}1)$$

Here h(n) is the impulse response.

Figure 3.3 shows the structure of FIR. The number of h[n-1] means n-1 orders or taps.
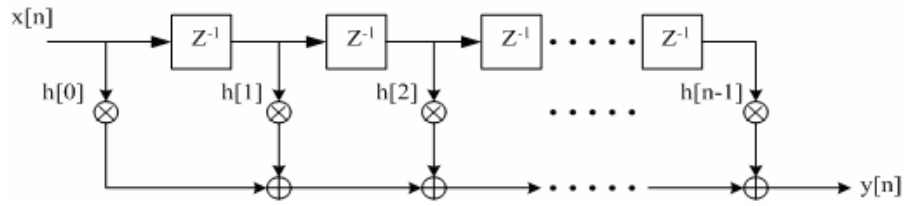
Figure 3.3 FIR structure

3.1.3 Implementation of interpolation filter

Half-band lowpass filter (HBF) is hardware efficient in reducing the circuit complexity in the design of a sharp cutoff FIR filter. Its coefficients are symmetric with respect to the center tap, and around 50 percent are zeros [4], which allows the reduction by half of the required multiplication. The ripple in passband and attenuation in stopband should be also properly set to avoid a huge computation and complex hardware.
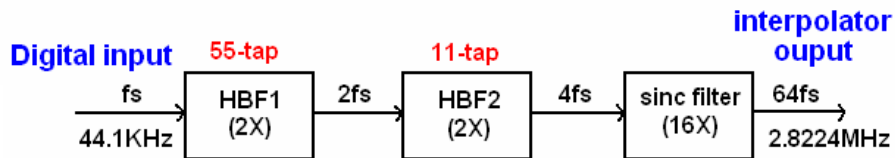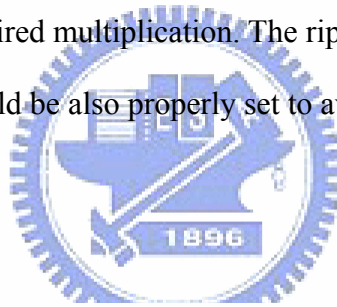
Figure 3.4 Implemented interpolator

Using a single upsampler and a single lowpass filter often leads to the high computation complexity [4]. An efficient realization of the interpolation filter was realized with as a cascade of several stages, to avoid the high computation complexity. Figure 3.4 shows the designed interpolator. The first half-band FIR filter (HBF1) is the most complex one to be designed (55-tap) since the transition band for this filter is often very small. The second half-band FIR filter (HBF2), larger transition bands

make their order much smaller (11-tap). Each HBF coefficient was quantized to the sum of a few integer powers of two, and represented by a canonic signed digit (CSD). The CSD allows encoding a binary number such that it contains the minimum possible number of non-zero bits [5]. The complex multiplication with filter coefficient is thus replaced with a few shift-and-add operations without multiplier. Finally, the last stage of the interpolation filter is often implemented by using a digital sinc filter whose transfer function is given by [6].

$$H(z) = (\frac{1}{L}\frac{1-z^{-L}}{1-z^{-1}})^K \qquad (3\text{-}2)$$

Where L is the interpolation factor.

Figure 3.5 shows the architecture of implemented second half-band FIR filter [7].
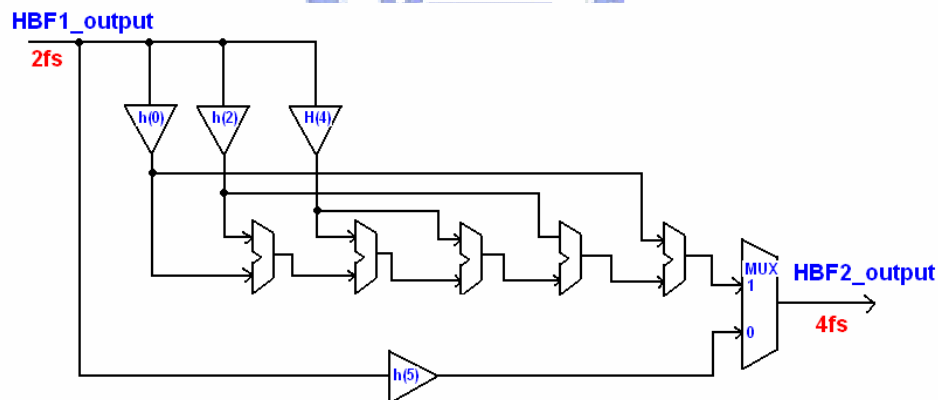
Figure 3.5 Second half-band FIR filter

Figure 3.6 shows the frequency responses of the first and second stage HBFs.
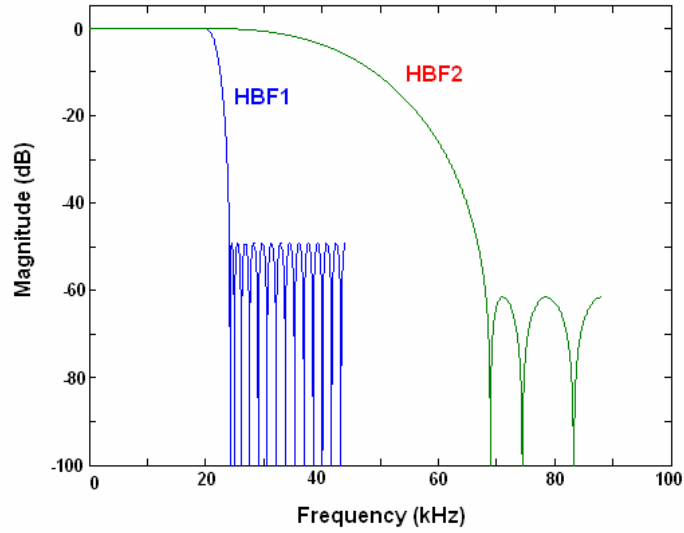
Figure 3.6 Frequency responses of HBF1 and HBF2

Table3.1 shows the quantized filter coefficients in CSD for the second HBF.

Coeffieient		Value	CSD	Relative Error(%)
h(0)	**h(10)**	0.011271925730837	$2^{-6} - 2^{-8} - 2^{-11} + 2^{-15}$	**0.09704998**
h(2)	**h(8)**	-0.060993672848504	$-2^{-4} + 2^{-9} - 2^{-11} + 2^{-14} - 2^{-16}$	**0.00703837**
h(4)	**h(6)**	0.300138840066905	$2^{-2} + 2^{-4} - 2^{-6} + 2^{-8} - 2^{-10}$ $+2^{-12} + 2^{-14} + 2^{-16}$	**0.00457055**
h(5)		**0.5**	2^{-1}	**0**

Table 3.1 quantized filter coefficients in CSD for the second HBF

Figure 3.7 shows the architecture of implemented sinc filter.

$$H(z) = (\frac{1}{L}\frac{1-z^{-L}}{1-z^{-1}})^K$$

L=16
K=3
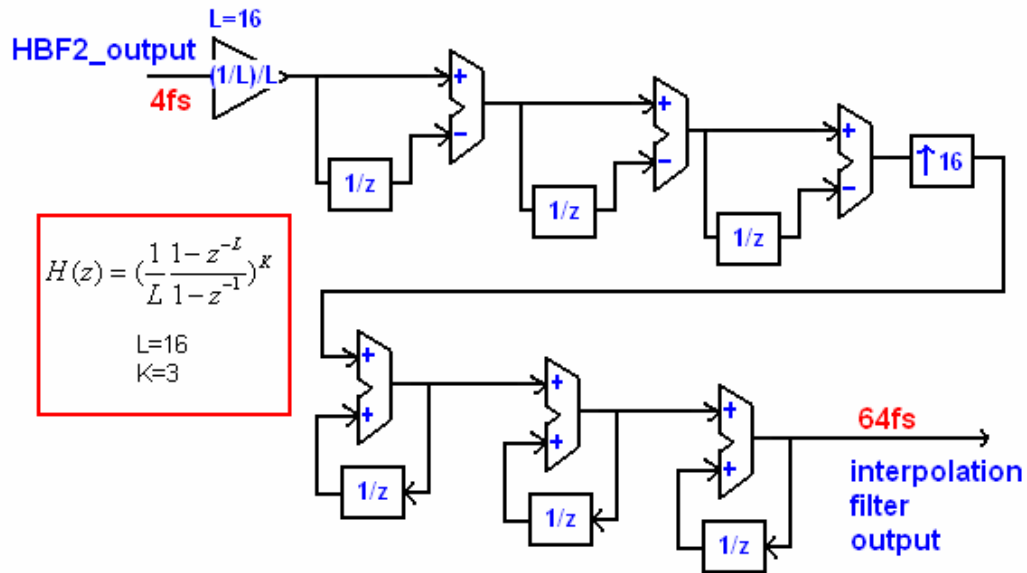
Figure 3.7 Implemented sinc filter

Figure 3.8 shows the frequency response of sinc filter.

X: 0.1777
Y: -39.45
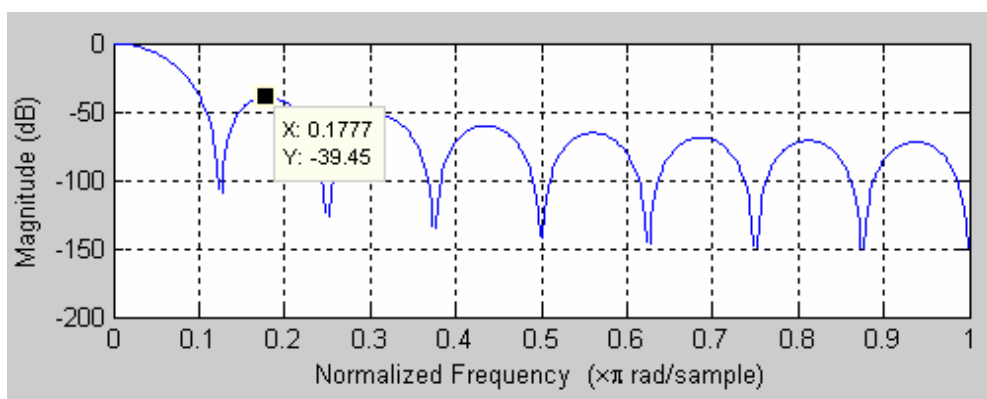
Figure 3.8 Frequency response of sinc filter

Figure 3.9 shows the frequency response of interpolation filter after synthesis.
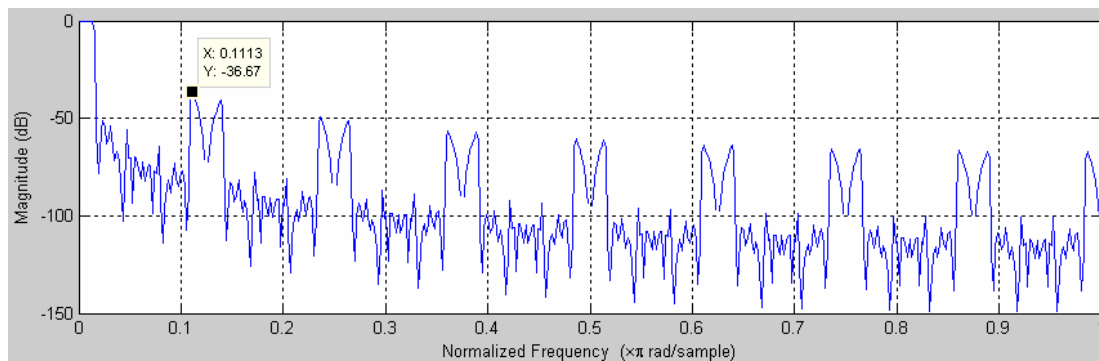
Figure 3.9 Frequency response of interpolation filter after synthesis

The interpolation filter is composed of two cascaded half-band FIR filters, followed by a digital sinc filter. It interpolates by the oversampling ratio (OSR=64), and achieves more than 36.67dB attenuation in the stopband and less than $\pm 0.03 dB$ ripple in the passband. The first two HBFs increase the OSR to 4, and the last sinc filter further increases the OSR by 16 times, to provide the overall OSR of 64. The orders of the two half-band FIR filter stages are 54 and 10. Thus, the numbers of realized distinct nonzero filter coefficients for these filters are 15 and 4.

3.2 Delta sigma modulator design

At the output of the interpolation filter, a delta-sigma modulator with third-order, CIFF (cascaded integrated feedforward) structure is shown in Figure 3.10 [6]. For accumulators in the CIFF structure, less bits are required to achieve the desired SQNR, because it only processes the errors between the input and the output. It is this property that makes it less susceptible to coefficients truncation than that of the competing architectures.
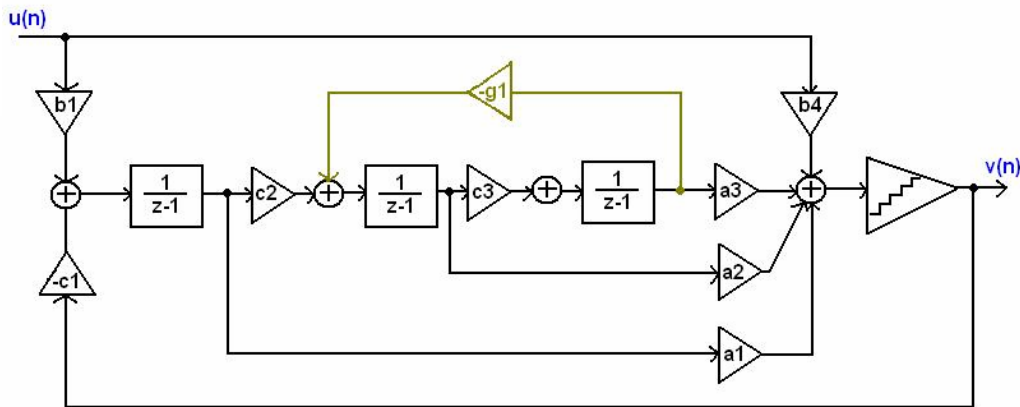
Figure 3.10 Delta-sigma modulator architecture

Table 3.2 Modulator specifications

Parameter	Value
Input sampling rate	2.8224MHz
Signal bandwidth	20kHz
Signal-to-noise ratio	120dB
Modulator sampling rate	2.8224MHz
Internal DAC levels	15

Table 3.3 Modulator coefficients

Coefficients	Value
a1	1/2+1/16
a2	1/2+1/16
a3	1/2-1/16
b1	1
b4	1/2
C1	2
c2	1/2
c3	1/4
g1	1/256+1/512
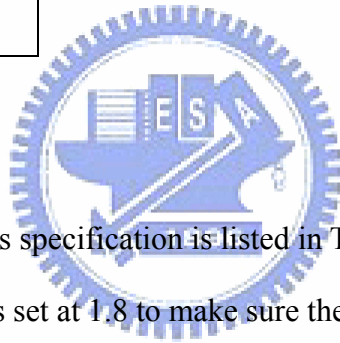
The designed modulator's specification is listed in Table 3.1. The maximum out-of-band gain of NTF was set at 1.8 to make sure the loop was stable (<2). The coefficients for the modulator were obtained by using delta-sigma toolbox [8] and are given in Table 3.2. The local feedback path (-g1) minimizes the in-band quantization noise in the modulator loop by placing two complex-conjugate zeros close to the edge of the signal band.

If N_1, N_2, N_3 are required to quantize the first, second, and third accumulator in the modulator loop, for a desired SNR better than 120dB caused by the finite word length of the accumulator and a full-scale sine wave with power of $M^2/2$, N_1, N_2 and N_3 are given by

$$\frac{1}{b1^2} \frac{(2^{-N_1})^2}{3} \frac{1}{OSR} < 10^{-12} \frac{M^2}{2} \tag{3-3}$$

$$\frac{1}{(b_1 c_2)^2} \frac{(2^{-N_2})^2}{3} \frac{\pi^2}{3(OSR)^3} < 10^{-12} \frac{M^2}{2} \tag{3-4}$$

$$\frac{1}{(b_1 c_2 c_3)^2} \frac{(2^{-N_3})^2}{3} \frac{\pi^4}{5(OSR)^5} < 10^{-12} \frac{M^2}{2} \tag{3-5}$$

Solving eq (3-3), (3-4) (3-5) gives $N_1 = 12.732$, $N_2 = 8.5912$, $N_3 = 5.8742$. [6]

Therefore, it is required to use 13, 9, 6 bits for the first, second, and third accumulator in the modulator. The resulting output waveform and spectrum of the delta-sigma modulator are shown in Figure 3.11 and Figure 3.12 respectively. The out-of-band spectrum is shown in Figure 3.13. As expected in delta-sigma modulator, a significant out-of-band noise is presented.
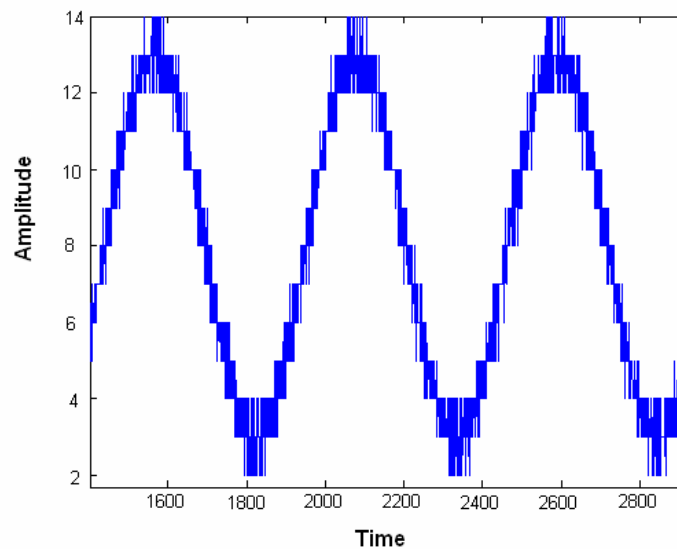
Figure 3.11 Output of the modulator
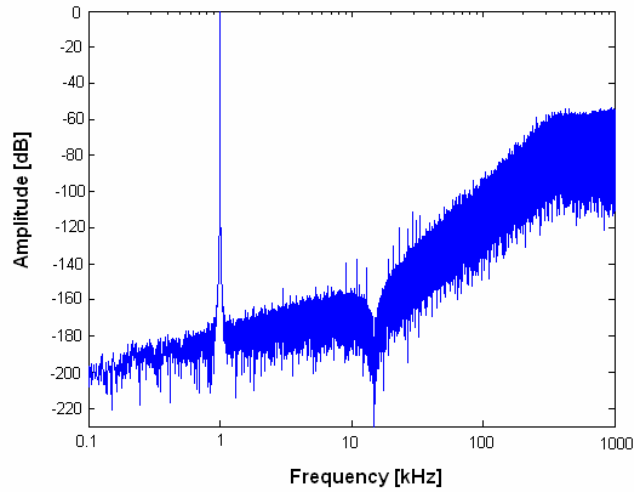
Figure 3.12 Output spectrum of the modulator
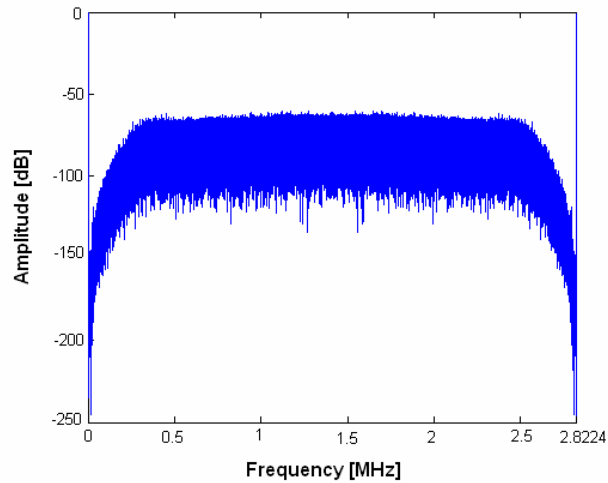
Figure 3.13 out-of-band spectrum of the modulator

The use of the multibit quantizer can also make the structure of the delta-sigma modulator more stable. However, the multilevel output requires using a number of unitary components at the digital-to-analog interface (i.e. capacitors), which is equal to the number of the quantizer output levels. The natural mismatches between the analog devices cause signal distortion. This problem can be solved by implementing dynamic element matching (DEM) at the digital-to-analog interface.

3.3 Dynamic Element Matching

A dynamic element matching (DEM) algorithm is to execute the randomized selection of the analog elements [9], [10]. It can avoid performance loss in terms of SNR and THD (total harmonic distortion) due to the mismatches between the capacitors, which is used in the input structure of the reconstruction filter. The noise due to distortion may be translated to white noise or shaped in spectrum depending on the used algorithms. For example, it may be a highpass characteristic. The randomized selecting process is realized in two stages, which are thermometer encoder and DWA (data weighted averaging) encoder [11]. They are shown in Figure 3.14. The 4-bit signal of the delta-sigma modulator output is translated into 15-bit signal by a thermometer encoder. Then this 15-bit signal is randomized by a DWA encoder.
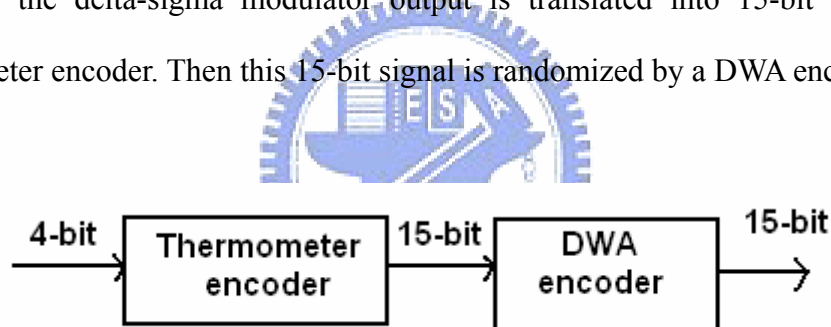
Figure 3.14 The implementation of DEM process

3.3.1 Thermometer code encoder

The operation of thermometer encoder is to convert binary into thermometer code, with the lower ranks producing all ones, and the higher ranks producing all zeros. Then how many capacitors of the digital-to-analog interface must be charged depends on the thermometer code. This thermometer encoder is used to transfer the four signed bits of the delta-sigma modulator output signal. The four signed bits means the levels from -8 to +7. The translation results are listed in Table 3.4.

Quantizer levels	Logic word or Number of selected capacitors	Thermometer word
+7	15	111111111111111
+6	14	011111111111111
…	…	…
1	9	000000111111111
0	8	000000011111111
-1	7	000000001111111
…	…	…
-7	1	000000000000001
-8	0	000000000000000

Table 3.4 Operation of thermometer encoder

Note that no charge has to be injected in the analog reconstruction filter when the 0 logic level is chosen, so no input capacitors are selected.

3.3.2 DWA (data weighted averaging) circuit

The DWA algorithm uses all the internal DAC components of the analog reconstruction filter at the maximum possible rate while ensuring that each component is used the same number of times. This is realized by selecting components sequentially from an array, and then beginning with the next available unused component. Figure 3.15 illustrates the concept for a 3-bit DAC with an input sequence of 2, 4, 7, and 5. A 3-bit DAC can be translated into 7-bit thermometer code and

implemented by seven equally weighted elements. The first two elements of the DAC are selected when the input sequence, 2(1100000), is applied. The next four elements of the DAC are selected when the input sequence, 4(0011110), is applied. If the input sequence, 7(1111111), is applied, all elements of the DAC are selected. When the next input sequence, 5(1111001), is applied, the first four and the last one are selected. The component selection will continue in this manner sequentially as the input data is applied.
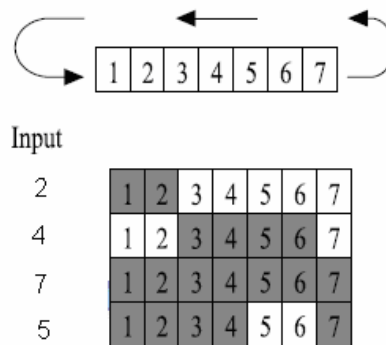
Figure 3.15 DWA operation

As described above, the element averaging is controlled entirely by the input data sequence. Thus, we can refer it to data weighted averaging (DWA) dynamic element matching. This element selection process can use all elements at the maximum possible rate, which ensures that the mismatch errors between components will sum to zero quickly, moving distortion to high frequencies. Another consequence of the cyclic sequencing is that no element of the DAC is selected with an inordinate numbers of times, even in a short time interval. A 15-bit internal DAC is adopted for this design. The input data is 15-bit thermometer code translated from the 4-bit data of the delta-sigma modulator output. The components of the DAC are selected according to the method described above.

Implementation of the Analog circuits in $\Delta\Sigma$ DAC design

4.1 DAC circuits

The block diagram of the analog part circuit is shown in Fig 4.1, which consists of internal DAC and post filter. The function of the internal DAC is converting digital signal input to analog signal output. And the function of the analog post filter is to smooth the digital signal and to reject the out-of-band noise, without compromising the signal purity achieved with the previous digital processing.
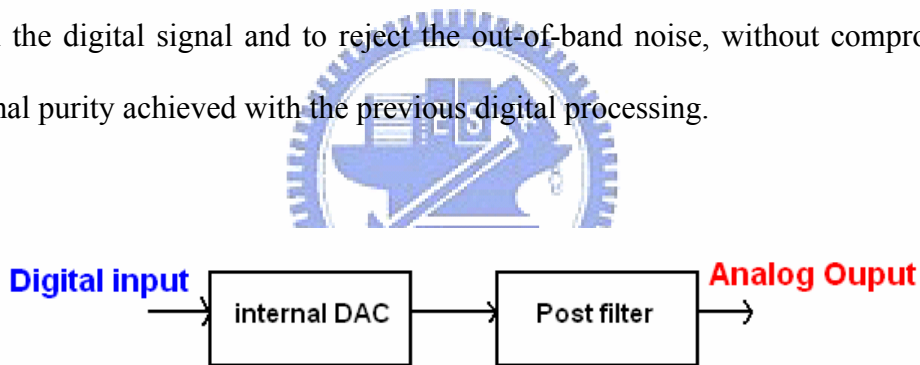
Fig 4.1 Block diagram of analog part circuit

The major concern in analog design is the minimization of power consumption and area size, while achieving the required DR (dynamic range) and SNR_{out} (out-of-band SNR). These two parameters refer to different aspects. The DR refers to the noise located in the signal band and is dominated by the 1/f and thermal noise of the analog part. The SNR_{out} refers to the residual noise out of the signal band and is dominated by the quantization noise, which depends on the amount of filtering section implemented in the analog part. The two parameters are in tradeoff: a larger amount of out-of-band filtering requires a larger analog filtering section and this causes higher

in-band noise, which reduce the DR. For the minimization of the power consumption and area size in addition to the low noise requirement, we realize the analog post filter with less operational amplifiers.[12]

4.1.1 Conventional Switched-Capacitor DAC

Figure 4.2 is a circuit diagram of a conventional switched-capacitor D/A converter. [13] The switched-capacitor D/A converter includes an operational amplifier. This amplifier is coupled to have a voltage follower function such that an output terminal of the amplifier is connected to an inverting input terminal. During ϕ_1 phase, switches S1 and S2 enter a closed state and the capacitor Cin is discharged by connecting to the ground. During ϕ_2 phase, the switches S1 and S2 enter an open state. At the same time, due to the operation of the switch S3, and depending on the polarity of the digital data. The output is charged.
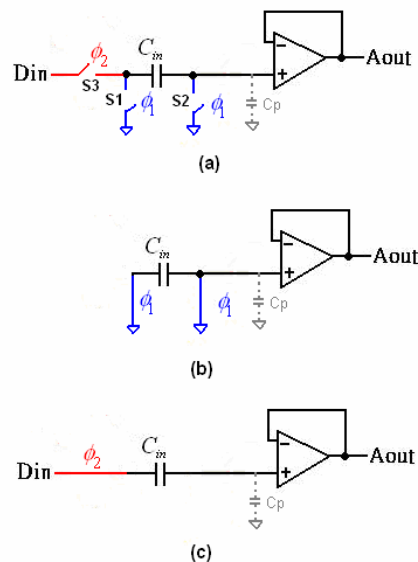
Fig 4.2 (a) Conventional SCDAC1 (b) during ϕ_1 phase (c) during ϕ_2 phase

Typically, a parasitic capacitance Cp is present at non-inverting input of amplifier. Parasitic capacitance is inherent in the manufacture and operation of the switching node. As a result, parasitic capacitance Cp will cause a large error to DAC's output.

   In order to solve the problems arising in figure 4.2, a switch capacitor D/A converter as shown in fig 4.3 may be used [13]. During the sample phase ϕ_1, capacitors C_{in} sample the data of the digital output. Shorting the input and output terminal causes the electric charge on the feedback capacitor Chold becomes zero. During integrating phase ϕ_2, the output is charged. Since the inverting input terminal is always in the virtually grounded condition, the charge stored in the parasitic capacitor when ϕ_1 is at the high level is equal to that stored in the parasitic capacitor when ϕ_2 is at the high level. The overall result is there is no parasitic capacitance added to the inverting input. However, this type of SCDAC has unacceptably large power consumption because the amount of charge to be supplied by the opamp.

(a)

(b)

(c)
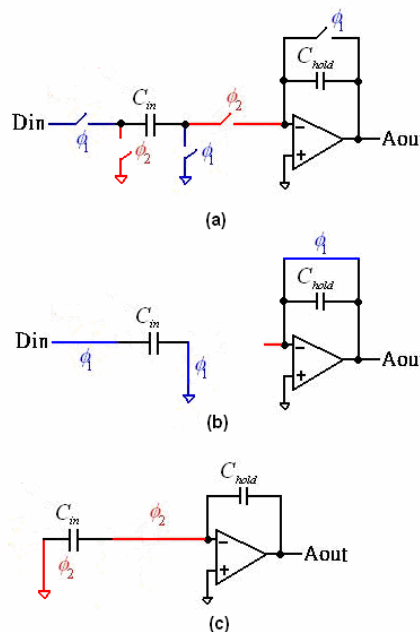
Fig 4.2 (a)Conventional SCDAC2 (b) during ϕ_1 phase (c) during ϕ_2 phase

4.1.2 SC DAC using Direct-Charge-Transfer technique

In a conventional SC DAC, an increase of capacitor size in attempt to reduce kT/C
noise requires a corresponding increase of power consumption. Using the DCT-SC
(direct charge transfer switched-capacitor) technique makes its power dissipation less
dependent on capacitor size [14]. This technique was originally proposed to realize a
robust unity gain amplifier and was later adopted to prevent the problem of opamp
slew limiting at the switched-capacitor to continuous-time interface in the analog
reconstruction filter of a 1-bit DAC. Slew limiting in the opamp results in a spike in
stair step waveform, which causes distortion when it is filtered in continuous-time.
The concept of an internal DAC with DCT-SC technique is shown in Figure 4.4.
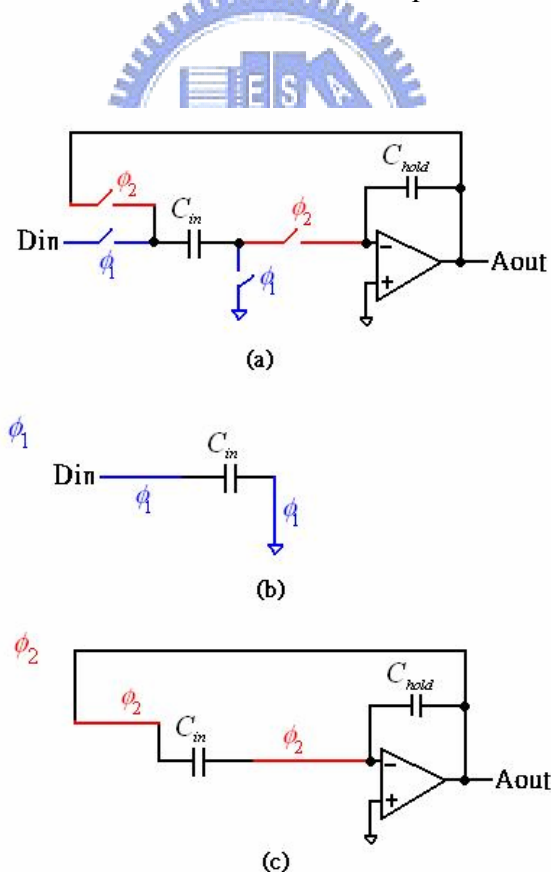
Figure 4.4 Concept of the DCT-SC technique [14]

During the sample phase ϕ_1, capacitors C_{in} sample the data of the digital output. During the hold phase ϕ_2, the top of C_{in} is connected to the inverting input of the opamp and the bottom plates are all connected to the opamp output. By this operation, the charge sampled at ϕ_1 will be distributed averagely by direct charge transfer among the capacitors at ϕ_2. Therefore, the analog output level is generated without the support of the opamp. Since the input capacitor C_{in} directly transmits the charge to the integrating capacitor C_{hold}, the opamp does not need to provide charging current for the capacitors.

The use of DCT technique makes the slew component of power consumption negligible and independent of capacitor size, because the power required charging the bottom plate parasitic capacitance mostly determines the power consumption. Hence this reason allows use of larger sampling capacitors for resisting noise with small increase of power consumption. At the discrete-to-continuous-time interface, any nonlinearity of the analog output waveform will be converted into noise or distortion in the following lowpass filter. By use of SC technique, clock jitter does not affect the analog levels of the discrete-time sampled points if the settling is adequate. However, when observed in continuous-time, clock jitter appears as a random signal which causes the stair step waveform of the output. The output signal includes high frequency quantization noise, which will be modulated into the signal band. Fortunately, the integrating capacitor C_{hold} provides a first-order lowpass characteristic with a cutoff frequency about 170 kHz in addition to the DAC function. This reduces the high frequency quantization noise and the noise modulated back to the signal band.

4.1.3 Other examples of DAC circuits

An example of 5-bit SC DAC with hybrid post filter is shown in Fig 4.5 [15]. Each capacitor array consists of 31 unit capacitors, C_1 to C_{31}. During the sampling phase ϕ_1, they sample the data which comes from DWA (digital) output. During the integrate phase ϕ_2, all capacitors are connected in parallel between the summing node and opamp output. The output level is generated passively by distributing the charge in the feedback path. Each half of the differential circuit has two capacitor arrays. One is controlled by the DWA output data, and the other by data delayed one cycle. This realizes the two-tap FIR filter with $1 + z^{-1}$ transfer function. The feedback capacitor C_{FB} provides a first-order LPF function. The cut-off frequency is determined by the ratio between C_{FB} and $C_{sampling}$.
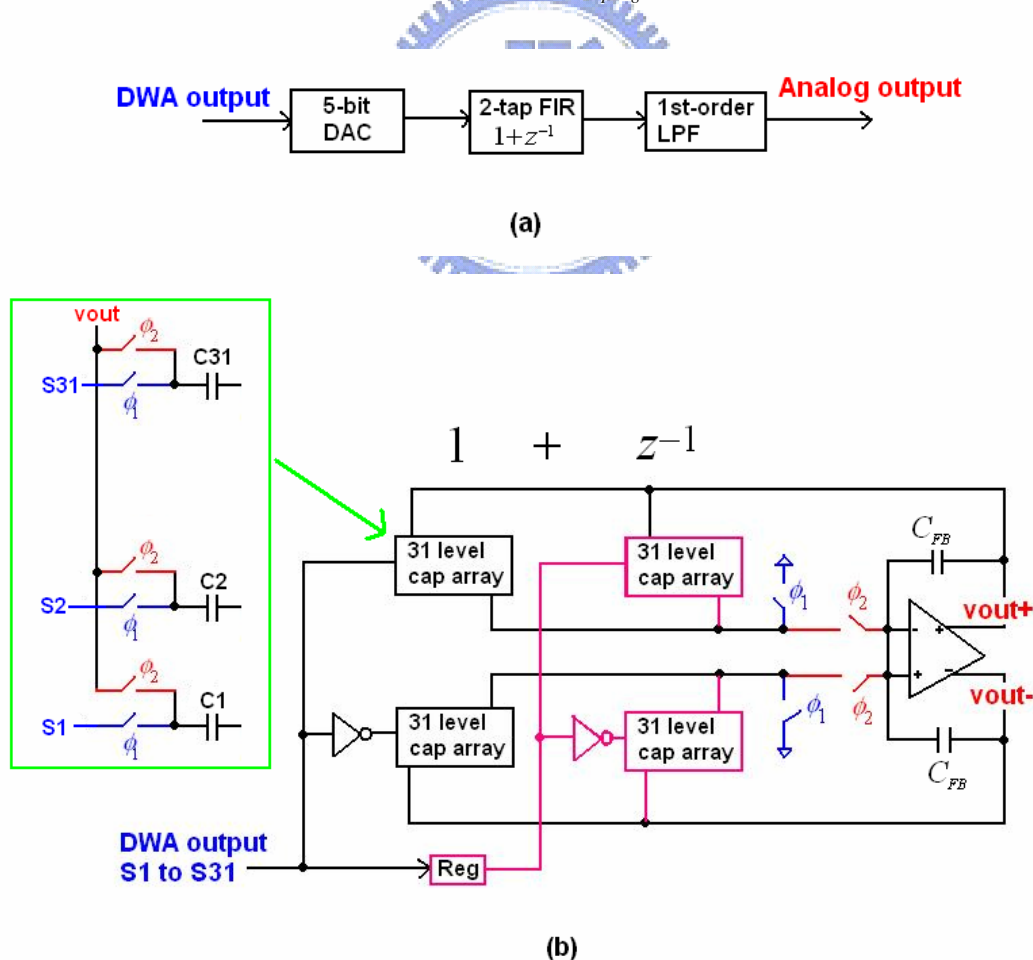
Fig 4.4 Five-bit SC DAC with hybrid post filter [15]

Another analog part circuit for ΔΣDAC, described in [16], used a 13-level truncation. Its Switched-Capacitor Filter was a third-order Chebyshev filter. This saved one amplifier. It is shown in Fig 4.6 as a single-ended circuit (the actual implementation was fully differential). During the sampling phase, an array of twelve unitary capacitors is switched to VDD or ground according to the related code coming from the ΔΣ modulator, while during the integration phase, all the capacitors are connected in parallel between the first opamp input node and the SC filter output. Third-order SC Chebyshev filter was used to strongly reduce the out-of-band noise and a 1st-order continuous time filter was then followed.
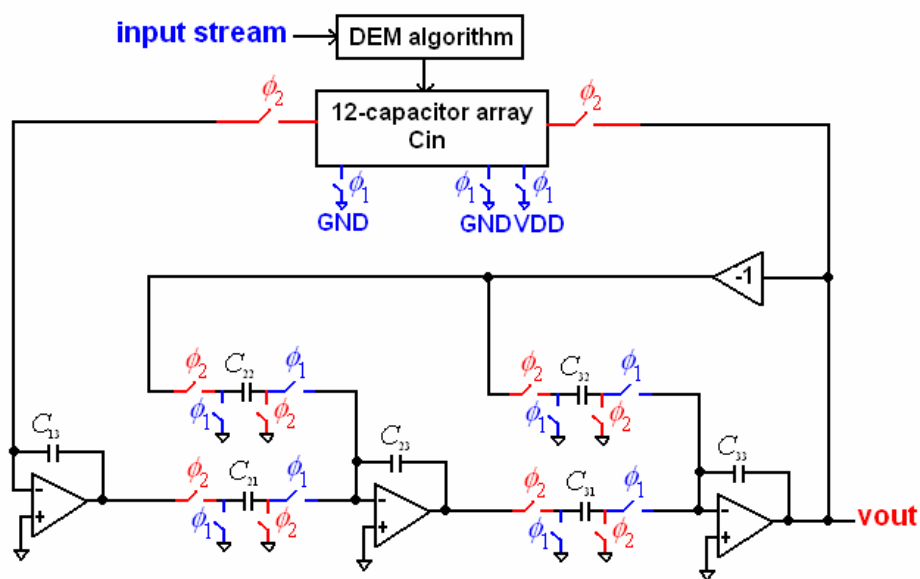
Fig 4.6 Third-order SC reconstruction filter [16]

Third example, an audio DAC is realized by using an SC array to transfer the sampled charges directly into the integrated headphone driver [17]. Thus, the DAC and the driver can all be combined, and need only one opamp. Fig 4.7(a) shows the second-order Sallen-key filter which is commonly used as the reconstruction filter in

audio delta-sigma DACs. The DAC output is applied to this filter to remove out-of-band noise. In this system, the input resistor R_1 is replaced by a SC structure as shown in Fig 4.7(b). By digitally controlling the SC branch, it can be used to perform the DAC function, saving hardware.

(a)

(b)

(c)
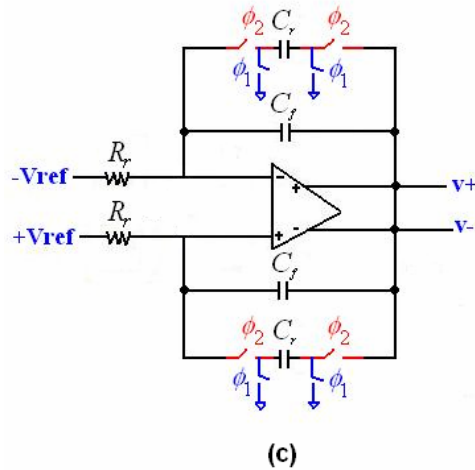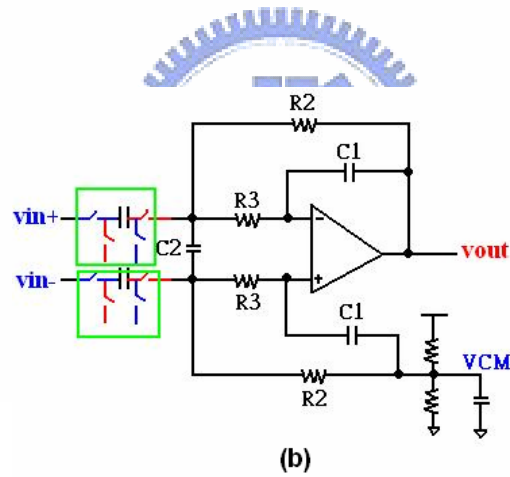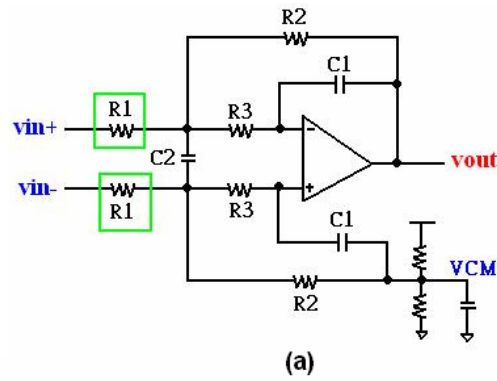
Fig 4.7 DAC stages (a) Conventional Sallen-Key filter (b) SC realization (c) Correction stage [17]
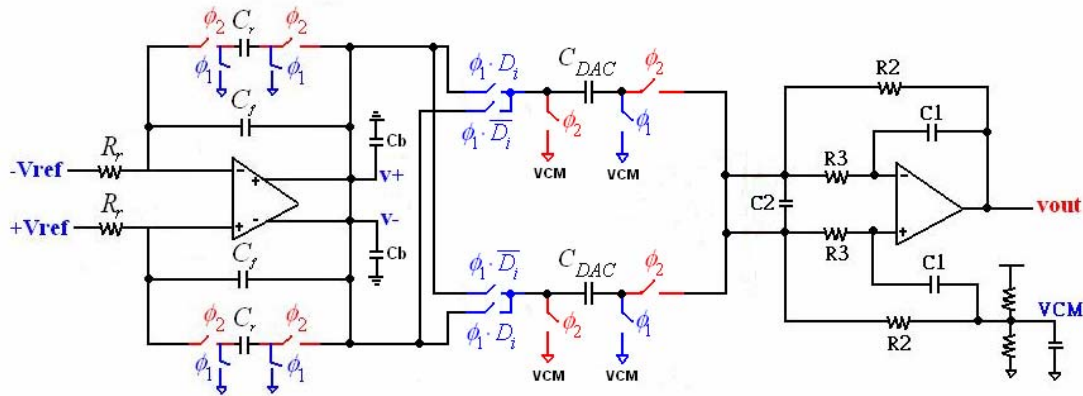
Fig 4.8 Gain-corrected DAC [17]

A problem with this new configuration is that the dc gain of the DAC is poorly controlled. The transfer function of the traditional Sallen-Key filter is given by

$$H(s) = \frac{-R_2 / R_1}{2 \cdot R_2 R_3 C_1 C_2 \cdot S^2 + (R_2 + R_3 + R_2 R_3 / R_1) \cdot C_1 \cdot S + 1} \qquad (4\text{-}1)$$

The dc gain of the filter is thus given by the ratio of R_2 and R_1, which is well controlled on chip. However, in the modified structure, the amplitude A of the filter output signal at dc is given by

$$A = 2 \cdot n \cdot V_{rsc} \cdot R_2 \cdot C_{DAC} / T_1 \qquad (4\text{-}2)$$

Here, V_{rsc} is the reference voltage sampled by the SC array, n is the number of the unit elements in the SC array and T_1 is the clock period in the DAC. Eq (4.4) shows that amplitude A depends on the time constant $R_2 \cdot C_{DAC}$ which is poorly controlled on chip. To control the amplitude A accurately, a gain correction stage was introduced, as shown in Fig 4.6(c). In steady stage, the dc currents entering nodes A and B through the resistive and SC branches equal zero. The output voltages are then given by

$$V^{+} = +V_{ref} \cdot T_2 / (R_r \cdot C_r) \qquad (4\text{-}3)$$

$$V^{-} = -V_{ref} \cdot T_2 / (R_r \cdot C_r) \qquad (4\text{-}4)$$

Here, T_2 is the clock period in the correction circuit. This stage generates the reference voltage for the DAC output stage. Combing (4.4), (4.5) and (4.6) gives

$$A = 2 \cdot n \cdot V_{rsc} \cdot (T_2 / T_1) \cdot (R_2 / R_r) \cdot (C_{DAC} / C_r) \qquad (4\text{-}5)$$

Eq (4-5) shows the amplitude A now depends on ratios of R and C values, which can be accurately controlled with careful layout.

Finally, an analog section of the DAC, which includes a resistor-array DAC (R-DAC), a second-order Sallen-Key low-pass filter, and the headphone driver is shown in Fig 4.9. In the resistor-array DAC, all switches are connected either to the high reference voltage or the ground. This avoids the problems with floating switches. An analog first-order FIR filter is also integrated into this DAC (d_i is delayed by one clock cycle with respect to b_i in Fig 4.8). This introduces a zero at one-half of the sampling frequency, and reduces the clock jitter sensitivity [18].
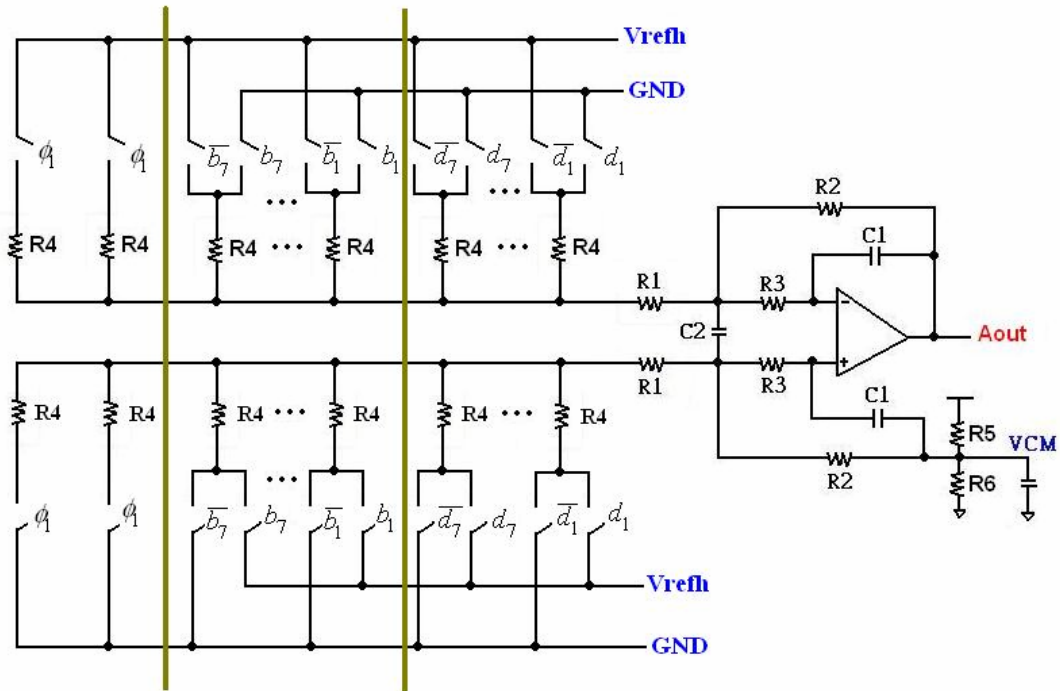
Fig 4.9 Resistor array DAC with first-order FIR filtering [18]

4-2 Low-voltage Circuit design issues

4-2.1 Floating Switch

Switches are affected by low supply voltage. Fig 4.10 shows the limitation on the operation of a floating switch in switched capacitor circuits. These limitations arise when the supply voltage is smaller than or equal to the sum of PMOS and NMOS threshold voltages $(V_{THN} + |V_{THP}|)$. If the power supply voltage, VDD is smaller then $(V_{THN} + |V_{THP}|)$, the switch will not be turned on even if the control signal voltage level of the NMOS is same as VDD or that of the PMOS is ground level. This is called the floating switch problem which is a serious concern in low-voltage switched-capacitor circuit design. The existing techniques that deal with this issue are discussed in the following section.
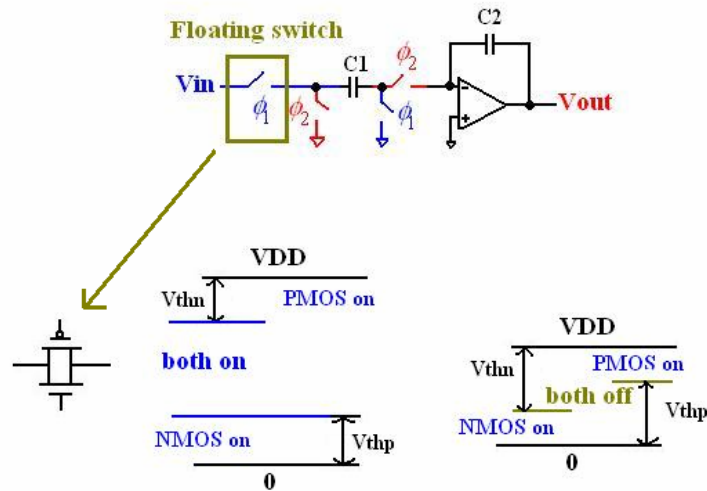
Fig 4.10 A SC integrator and the floating switch problem

4-2.2 Low-threshold Voltage Device

Lower threshold NMOS and PMOS transistors can be used at the expense of an extra mask layer for the CMOS process. It gives a simple and straightforward solution for the low-voltage SC circuit implementation, except for the extra cost of additional processing. However, the leakage current of MOS transistor with low threshold voltage limits the accuracy of charge transfer, and hence the effectiveness of this approach.

4-2.3 Clock voltage doubler

The clock voltage boosting technique increases the gate-source overdrive typically achieved by doubling the clock voltage applied to the gate of an NMOS floating switch. Fig 4.11 shows a clock boosting circuit proposed by Nakagome et al [19]. When the input signal is at VDD, capacitor C_2 is charged to VDD by connecting the inverted output level 0 to the bottom plate and VDD to the top plate. During this

phase, the output level of the boosted clock is lowered by turning off PMOS transistor M1 and turning on NMOS transistor M2. When the input signal is low, an inverted clock will pump the voltage at the top plate of C_2 to be almost 2VDD and PMOS device M1 will turn on to pass the boosted voltage to the gate of the floating switch MS. The peak voltage of the boosted clock signal is

$$V_{HI} = 2VDD \frac{C_2}{C_2 + C_p + C_{gate,MS}} \qquad (4\text{-}8)$$

Where C_p is the parasitic capacitance at the top plate of C_2 and $C_{gate,MS}$ is the gate capacitance of the floating switch MS. However, this approach introduces severe reliability issues in fine-line CMOS technologies due to the gate-oxide stress and p-n junction problems.
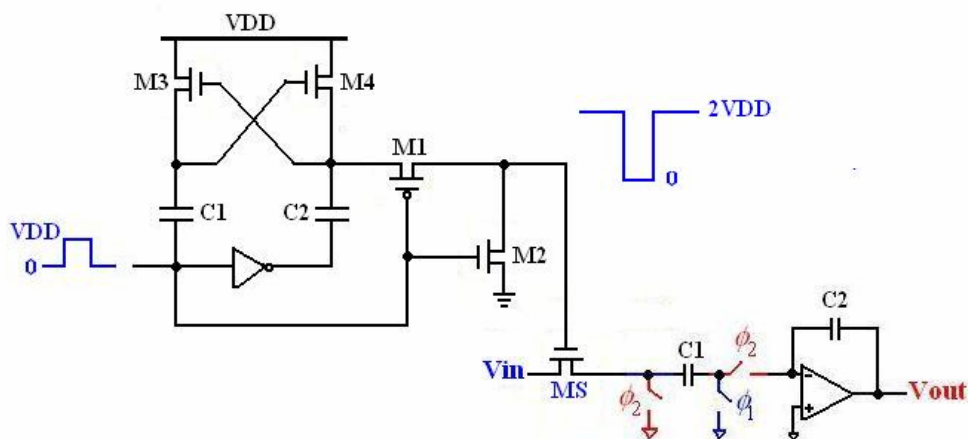
Fig 4.11 A clock voltage double circuit

4-2.4 Clock Bootstrapping

Clock bootstrapping technique [20] also enables a low-voltage switching operation using higher gate overdrive voltage. Linearity of the switch is also improved due to constant on-resistance resulting from constant V_{GS}. Fig 4.11 shows the basic concept of bootstrapped circuits. During ϕ_1 state, the capacitor is precharged to VDD. It will ideally act as a floating battery to bootstrap the gate voltage during ϕ_2 state. Assuming that the input terminal of the sampling switch is source, the "on" resistance is given by

$$Ron = \frac{1}{\mu_n C_{ox} \dfrac{W}{L}(V_{DD} - V_{tn})} \qquad (4\text{-}9)$$

Clearly, it is independent of input signal to reduce harmonic distortion. However, it requires separate bootstrapping circuits for each switch, resulting in more die area and power consumption.
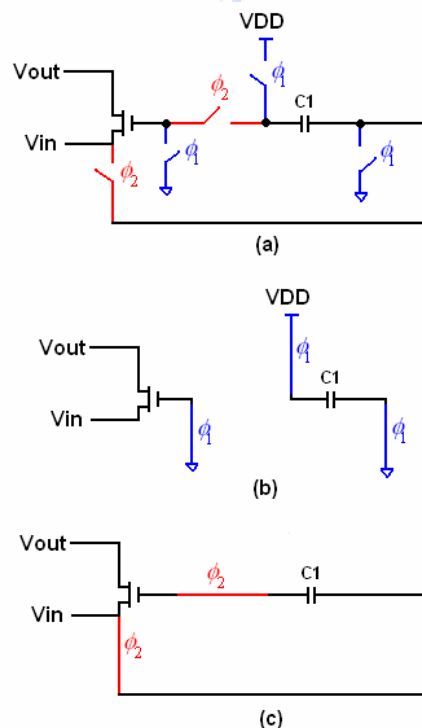
Fig 4.12 (a) Clock bootstrapped circuit (b) phase ϕ_1 (c) phase ϕ_2

4-2.5 Switched-RC technique

The switched-RC technique was proposed in [21]. In this scheme, the floating switch is replaced directly by a resistor as shown in Fig 4.13.
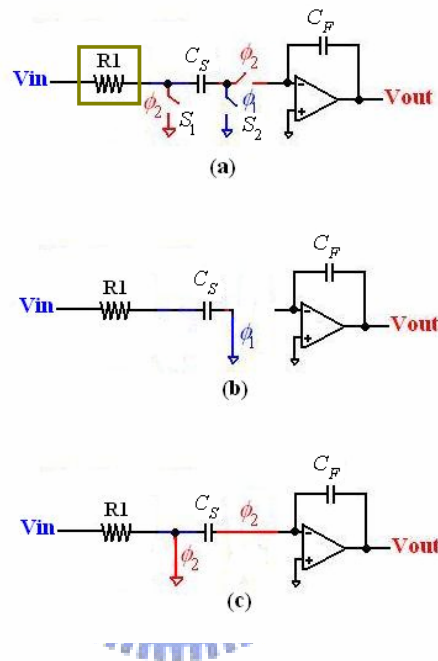
Fig 4.13 (a) Switched-RC Integrator (b) phase ϕ_1 (c) phase ϕ_2

This greatly improves the sampling linearity without using the clock bootstrapping. The integrator works as following : during clock phase ϕ_1 , capacitor C_S , samples the input through resistor R1, and switch S2, during clock phase ϕ_2 , charges stored in capacitor C_S , will be transferred to the integrating capacitor C_F . During the integrating phase, the resistor R1 and switch S1 will form a resistor divider through which the input signal will have a leakage at node X given by

$$V_X = Vin \frac{R_{ON}}{R_1 + R_{ON}} \qquad (4\text{-}10)$$

This input leakage at node X will result in a gain error which is given by

$$\frac{C_S}{C_F} \frac{R_{ON}}{R_1 + R_{ON}} Vin \qquad\qquad (4-11)$$

The ratio of R_{ON} and R_1 can be sized carefully to give a small gain.

4-3 Class AB amplifiers

The headphone driver is a key part in the audio applications which may define the performance of the overall system. A driver is an amplifier which can drive a low resistance and large capacitance load and has a small quiescent current. There are many different drivers (Class A, Class B, Class AB and Class D) that are classified according to their output stages and shown in Fig 4.14.
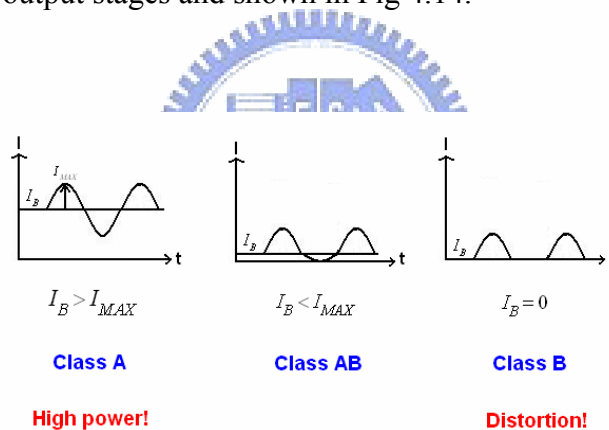
Fig 4.14 ClassA, AB, B output stages

A Class-A stage is a stage in which the peak current swing never exceeds the DC biasing current. The average current is therefore the DC current. In a Class-B stage the DC biasing current is zero. Connecting these swings to the negative swings from another amplifier leads to discontinuities, which is called crossover distortion. Class-AB amplifiers are somewhere in between. The DC biasing current (or quiescent current) is small compared to the peak current swings. It is well-known for its good linearity and power efficiency. Although Class-D output stage has higher power

efficiency and is used widely in audio application, it requires further off-chip filtering and has the IM signal around the switching frequency. Thus, it has greater noise as compared with the other amplifiers.

To deliver power to small resistors or large capacitors cannot be achieved with conventional output stages. The output currents are too large. For this purpose we need to bias the output stages in Class-AB. They have small quiescent currents but can deliver very large currents to the load.

4-3.1 CMOS output stage
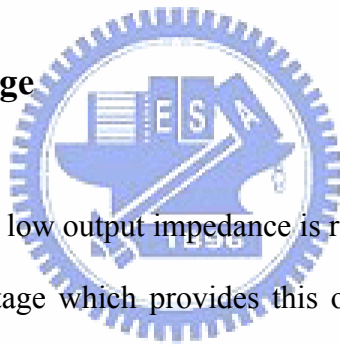
For a low-resistor load, a low output impedance is required. The source follower is the only simple transistor stage which provides this output resistance. However, its DC current handing is not sufficient. A source follower is shown in Fig 4.15, biased at 0.1mA. A low resistor of 50Ω is connected to it. It is clear that the maximum output voltage swing can only be 5mV. For higher output voltages, we would need higher biasing currents as well. This would lead to an excessive power consumption. We now need a transistor circuit which can deliver large currents only when needed, but with a low quiescent biasing current to lower the power consumption as much as possible.

If $I_B = 0.1mA$; $V_{out,peak} = 5mV_{peak}$

For $V_{out,peak} = 1V_{peak}$; $I_B = 20mA$

High power consumption !
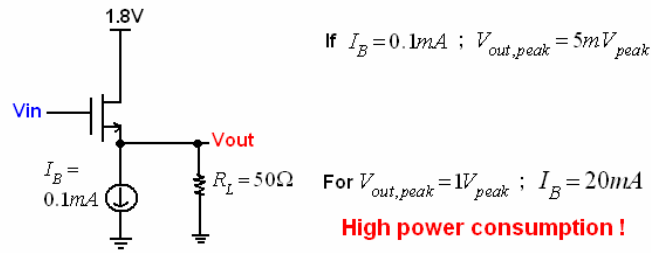
Fig 4.15 CMOS output stage problem

A possible solution is to have two source followers, Source to Source, as shown in Fig 4.16 (b). The current out of this stage can again be very large, depending on the transistor size. The PMOS can now be driven as hard as the NMOS. The main disadvantage of this double source follower is that the output swing can only reach the supply voltage within one V_{GSn}. Also, the output voltage can never be lower than V_{GSp}. For large supply voltages, there is no problem but for supply voltages of a few Volts, this is not acceptable. This is why most Class-AB output stages for low supply voltages have two output transistors Drain-to-Drain.

$V_{OUT} = V_{in} - V_{GS}$ **Push-Pull**   **Amplifier**
                              $V_{OUT,MAX} = V_{DD} - 2V_{GS}$ **Rail-to-rail**
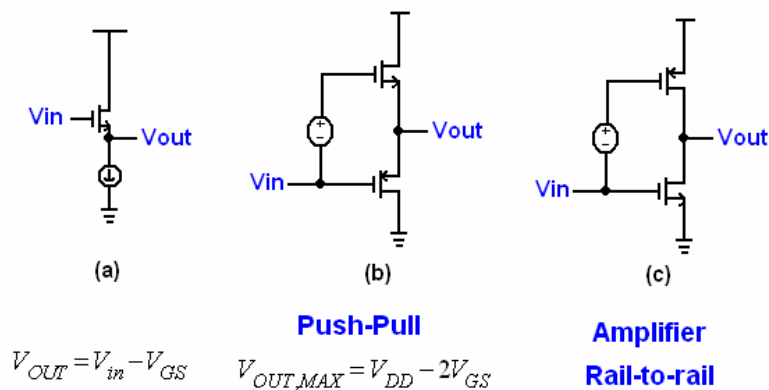
Fig 4.16 CMOS output stages

The basic requirement of class-AB stage is described as following. The first requirement is obviously that rail-to-rail swings are possible. The second one has indeed to do accurate control of quiescent current I_Q, it must be low and independent of supply voltage. Third, drive capability (defined as I_{MAX}/I_Q) must be as large as possible. The last specification has to do with complexity. Class-AB amplifiers are the most complicated DC-coupled amplifiers. Some simplicity is still welcome !

4-3.2 Cross-Coupled quads

A better class-AB amplifier is obtained by cross-coupling the input devices. In this way, a complementary differential pair can be constructed with an expanding characteristic. Figure 4.17 shows a simplified schematic of a cross-coupled class-AB amplifier which is proposed by Castello [22]. This circuit is perfectly symmetric. For zero applied differential input signal, the two matched current sources I uniquely define the circuit quiescent current level. In fact, if for simplicity it is assumed that the four NMOS input devices are identical, and the same is true for the four PMOS devices, then $I_1 = I_2 = I$. Furthermore since all current mirrors have a gain of 1, the quiescent current in the output branches is also equal to I. It follows, therefore that the quiescent power consumption in the circuit is precisely controlled by the two matched current source in the input stage. The dynamic behavior of the circuit is described as following.
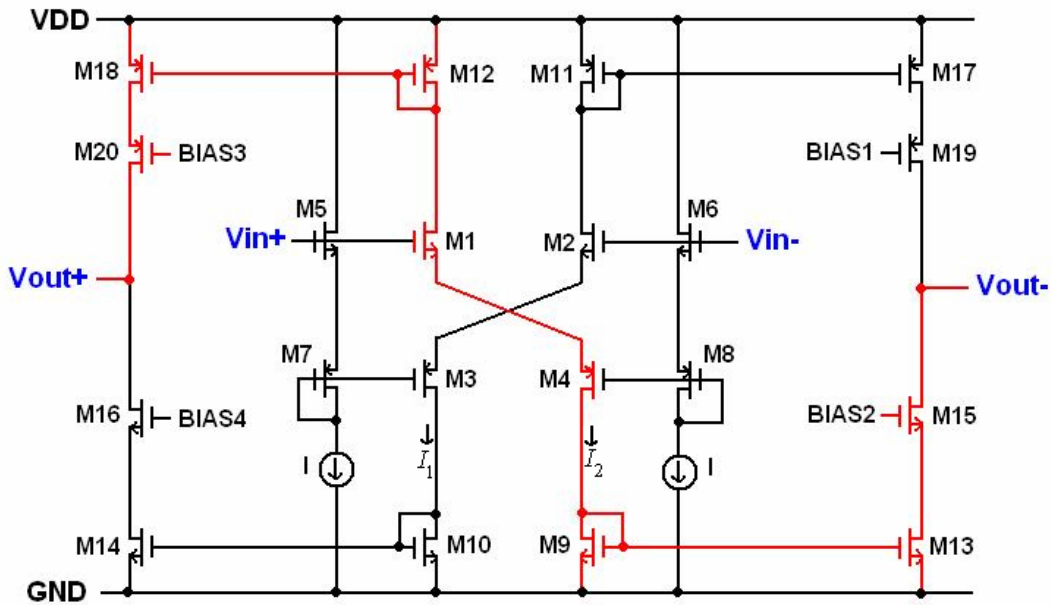
Fig 4.17 Castello's Cross-coupled Class-AB Amplifier [22]

In response to a large positive differential input signal, current I_1 goes practically to zero. As a consequence, half of the devices in the circuit become cut off. Current I_2, on the other hand, increases to a peak value which, in principle, is only limited by the value of the input voltage applied. The same current is mirrored to the outputs and can quickly charge and discharge the load capacitance. In simply, transistor M1-M4 form a cross-coupled input stage which split the input signal into two paths and provide the class-AB operation. M5-M8 and the two current sources (I) perform the level shifting and provide proper bias for the cross-coupled input devices. Transistors M9-M20 form four current mirrors which duplicate the currents of the input devices with a 1:1 ratio.

The same cross-coupling which is shown in Fig 4.18 is now used here in the output stage [23]. The cross-coupled pairs M13, M14, and M15, M16 provide an inherently symmetrical drive to the output transistors. The quiescent output current is a simple function of the current flowing through the level-shift transistors M17-M20, and the size ratio of these transistors to the cross-coupled pairs M13, M14, and M15,

44

M16. This current is multiplied by a factor of 10 in the output current mirrors
M21-M24.
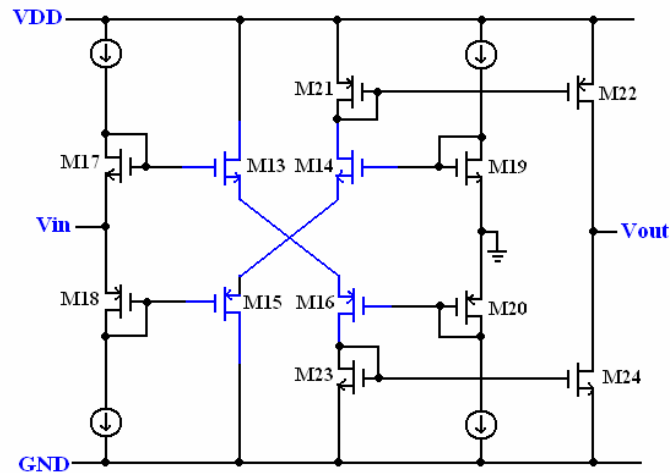
Fig 4.18 Fischer's Amplifier output stage [23]

The entire amplifier schematic is shown in Fig 4.19 [23]. A folded cascade input
stage has been modified by adding an additional input transistor pair in order to create
a symmetrical common-mode range. Assuming for the moment that node B is to be
tied to ground and no input voltage is applied when the amplifier is in closed loop,
symmetry dictates that node A will also be near ground. In this condition, the
drain-gate connection of transistors M17 and M18 has less than 0.5V overhead before
transistors M8 and M10 begin to leave the saturation region. This small voltage swing
is not enough to generate the large output currents required and also maintain a good
low-level bias. Therefore a matched load inverter M25-M28 is inserted between node
A and node B. This inverting buffer provide a gain of -1 at the expense of only four
transistors and effectively doubles the voltage drive to the cross-coupled pairs,
thereby maximizing the achievable current range.
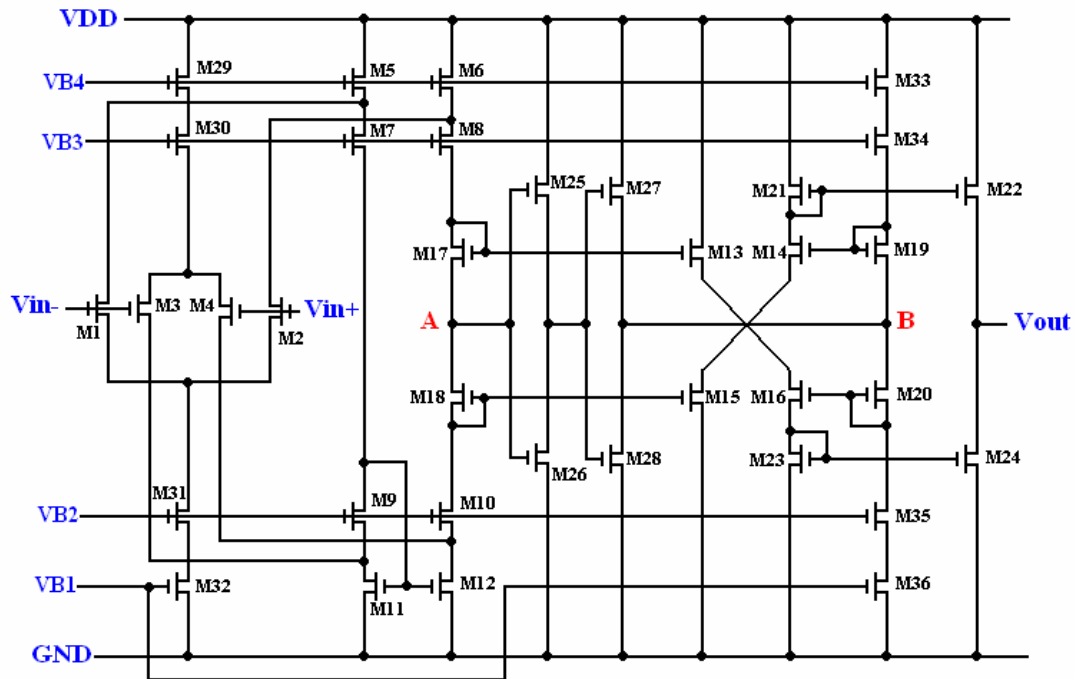
Fig 4.19 Entire Fischer's Amplifier schematic [23]

4-3.3 Adaptive biasing

Cross-coupled quads are a useful principle for generating expanding differential currents. It is not the only one however. Positive feedback can be used as well. Adaptive biasing is actually used. An adaptive biasing amplifier adapts its biasing to be able to provide larger output currents. The amplifier shown in Fig 4.20 is a symmetrical amplifier, which is single ended. Two times two current mirrors are added, i.e. with transistors M11/M12 and M13/M14. Without these transistors the maximum output current would be limited to BI_P.

In order to increase this maximum current, biasing current I_P must be made larger for larger input voltages. This biasing current is adapted to the input signal level. This is why it is in parallel with two more current mirrors through transistors M18 and M19. Let us follow the path to transistor M19.
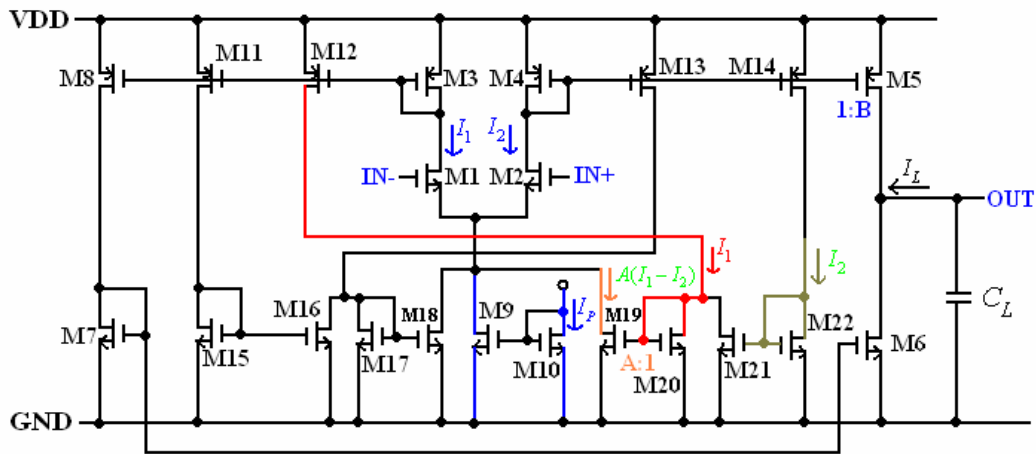
Fig 4.20 Adaptive Biasing Amplifier [24]

Transistor M19 forms a current mirror (with current factor A) with M20. This latter transistor take the difference in current $I_1 - I_2$, which are proportional to the currents in the input stage. The larger of these two currents wins. If I_1 is larger than I_2 then AI_1 current is added to I_P, increasing the total biasing current of the first stage, and also increasing the maximum output current. If, however, I_2 is larger than I_1, then it is mirrored by M17/M18, also multiplied by A and also added to I_P. This total biasing current increases in either direction. The amount of increase depends on current factor A. A disadvantage of this amplifier is that transistors M11-14 are added on the node where the non-dominant pole is formed. They will therefore slow down the amplifier. (dominant pole is formed by the high output impedance and a load capacitor, and the second pole is formed by the transconductance of the load transistors of the input stage and the internal capacitors)

4-3.4 I_Q control with translinear circuits

A Class-AB output stage can also be biased by translinear circuits. A translinear loop is a circuit which provides a linear relationship by use of nonlinear circuits. The simplest example is a current mirror. Both transistors have a nonlinear current-voltage relationship and yet the current gain is perfectly linear. The voltage between the two transistors is heavily distorted though.

An example which is proposed by Wu [25] is shown in Fig 4.21. A translinear

loop is formed by transistors MA2/MA4 and MA9/MA10. Their sum of V_{GS} 's is equal (Eq 4.5). The currents through MA9-MA10 are set by a DC current source (which is about $4\mu A$ in this example). The current through MA4 is also set by the DC current of the preceding stage (which is also about $4\mu A$ in this example). Only the current through the large output transistor MA2 is not known.

$$V_{GS2} + V_{GS4} = V_{GS9} + V_{GS10} \qquad (4\text{-}12)$$

$$I_{DS} = \frac{1}{2} k_p' (\frac{W}{L})(V_{GS} - V_{TH})^2 \quad (4\text{-}13) \quad \rightarrow \quad V_{GS} - V_{TH} = \sqrt{\frac{2I_{DS}}{k_p'(\frac{W}{L})}} \qquad (4\text{-}14)$$

Combine (4-12) and (4-14). All parameters V_{TH}, k_p' and constant cancel out.

$$\sqrt{\frac{I_{DS2}}{(\frac{W}{L})_2}} + \sqrt{\frac{I_{DS4}}{(\frac{W}{L})_4}} = \sqrt{\frac{I_{DS9}}{(\frac{W}{L})_9}} + \sqrt{\frac{I_{DS10}}{(\frac{W}{L})_{10}}} \qquad (4\text{-}15)$$

Table 4-1 Amplifier device size

Device	Size(μm)
MA2	$17 \times 160 / 2.4$
MA4	$2 \times 64 / 4$
MA9	$64 / 4$
MA10	$64 / 4$

As a result, we obtain an expression linking in Table 4-1.

$$(\frac{W}{L})_4 = 2(\frac{W}{L})_9 \qquad \text{and} \qquad (\frac{W}{L})_2 = 70.8(\frac{W}{L})_9 \qquad (4\text{-}16)$$

$$\sqrt{\frac{I_{DS2}}{(\frac{W}{L})_2}} = 2\sqrt{\frac{I_{DS9}}{(\frac{W}{L})_9}} - \sqrt{\frac{I_{DS4}}{(\frac{W}{L})_4}} = 2\sqrt{\frac{I_{DS9}}{(\frac{W}{L})_9}} - \sqrt{\frac{I_{DS9}}{2(\frac{W}{L})_9}} = \sqrt{\frac{I_{DS9}}{(\frac{W}{L})_9}}(2 - \frac{1}{\sqrt{2}}) \qquad (4\text{-}17)$$

$$\therefore \frac{I_{DS2}}{I_{DS9}} = \frac{(\frac{W}{L})_2}{(\frac{W}{L})_9}(2 - \frac{1}{\sqrt{2}})^2 = 118 \qquad (4\text{-}18)$$

The current I_{DS2} through transistor MA2 is about 120 times larger than the current

through transistor MA9. It is now well defined. It is independent of the supply voltage. The current through MA9/MA10 comes from a DC biasing current mirror. The DC current through MA4 comes from the PMOS differential current amplifier M11-M14 at the end of the NMOS first stage. This current flows through the NMOS differential current amplifier M5-M8 at the end of the PMOS first stage.

Complementary output devices MA1 and MA2 are driven by complementary common-gate level shifters MA3 and MA4. During quiescent operation, both MA3 and MA4 are biased into a conducting state. The gate-to-source V_{GS} bias voltages of the output transistors are kept low to minimize quiescent power consumption. The exact bias levels are controlled by the reference voltages V_{B1} and V_{B2}. During a negative slewing period, the gate voltage of MA1 will be pulled high. Fixed gate potential V_{B2} will cause MA3 to cutoff. MA4 will carry the full bias current, driving its source and the gate of MA2 high, turning off MA2. Under the condition of strong sourcing, MA2 will be turned on, symmetrically repeating the above operation on the other side of the circuit. Ultimately the swing on the gate of MA1 (MA2) will reach a limit at $2V_{DS(SAT)}$ from the positive (negative) rail. This large drive swing to both output devices allows driving heavy loads close to the rails. After the slewing period, as the input signal returns toward zero, both MA3 and MA4 will turn on again and the circuit quickly settles to a quiescent stage.
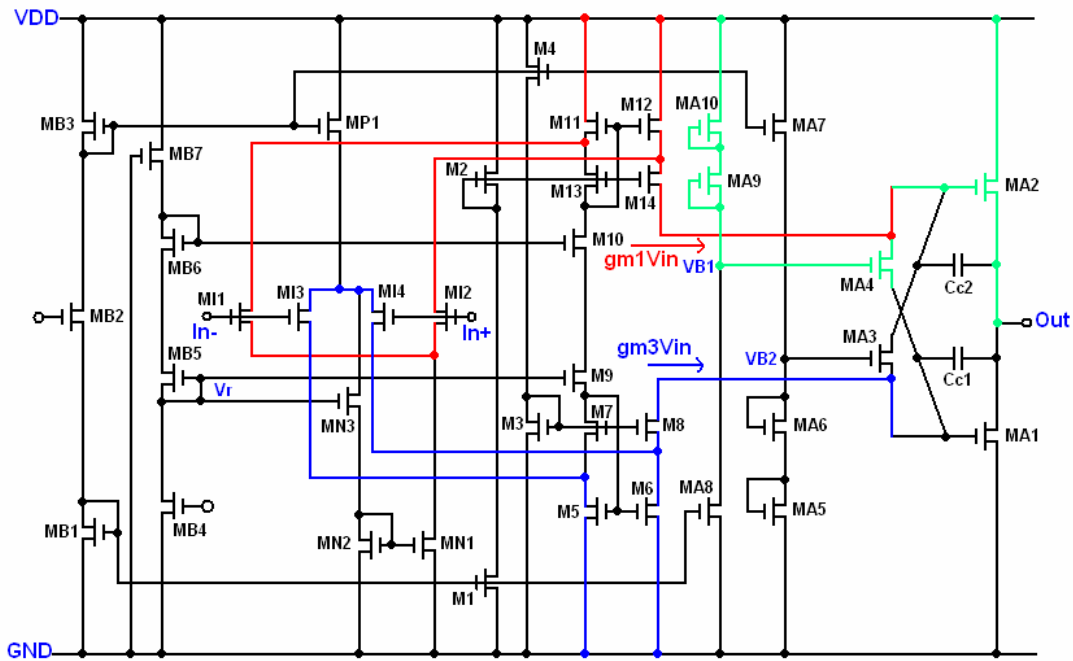
Fig 4.21 Wu's Amplifier [25]

This input stage is an improvement over the input stage of Fisher as the common mode voltage moves from the positive to the negative rail, the stage goes through three modes. First the PMOS devices are cutoff, then both device pairs operate, and finally the NMOS devices cutoff, during this time the input stage transconductance changes by a factor of 2. This requires excessive frequency compensation to ensure stability at all input levels.

The NMOS pair MI1, MI2, is biased by a current source MP1 via MN3 and the current mirror MN1, MN2, when the PMOS pair is nonconducting. When the common mode input voltage is at least equal the reference voltage V_r above V_{TH}. When the input CM voltage decreases through the reference voltage V_r, the source current is gradually steered from the source of MN3 to the PMOS pair, removing current from the NMOS pair. Since the tranconductance if MOS's are proportional to the square root of drain current, keeping the sum of the drain currents constant, the combined

transconductance variation of PMOS and NMOS pairs will be improved from a factor of 2 to a factor of $\sqrt{2}$ compared to the original circuit of Fisher []. To make the top PMOS cascade stage work symmetrically with the bottom NMOS stage it is employed a floating current source. Current mirrors are formed by MB6, M10 and MB5, M9. Transistors MB7 and MB4 act as resistors. The bias currents for the upper and lower cascade stages M11, M13 and M7, M5 are thus set equal. With proper selection of the ratio between MB5, M9 and Mb6, M10, we may set the reference current while maintaining node A and node B at the same potential.

A similar translinear loop to set the quiescent current through the output devices is found in Fig 4.22 [26]. The opamp contains a rail-to-rail input stage, M1-M4, with a g_m control by three-times current mirrors, M5-M10 and M29-M31, a summing circuit, M11-M18, and a class-AB output stage, M19-M26. The floating current source, M27-M28, biases the summing circuit and the class-AB control.

The rail-to-rail folded cascaded input stage can be biased either in weak or in strong inversion. If the input stage is biased in strong inversion, then the total g_m is given by

$$g_m = \sqrt{\mu_p C_{ox}(\frac{W}{L})_p I_p} + \sqrt{\mu_n C_{ox}(\frac{W}{L})_n I_n} \qquad (4\text{-}19)$$

From Eq 4-19, the transconductance can be made constant by keeping the sum of the square roots of the tail currents of the complementary input pairs constant. This yields

$$\sqrt{I_p} + \sqrt{I_n} = 2\sqrt{I_{ref}} \qquad (4\text{-}20)$$

Where it is assumed that the W over L ratios of the input transistors obey the condition

$$\frac{(\frac{W}{L})_p}{(\frac{W}{L})_n} = \frac{\mu_n}{\mu_p} \qquad (4\text{-}21)$$

The g_m of this input stage is regulated by means of two current switches, M5 and M8, and two current mirrors, M6-M7 and M9-M10, each with a gain of three. For the sake of simplicity, this current mirrors will be called three-times current mirrors, in the remaining part of this section. The sizes of the input transistors are chosen such that relation 4-21 is obeyed.
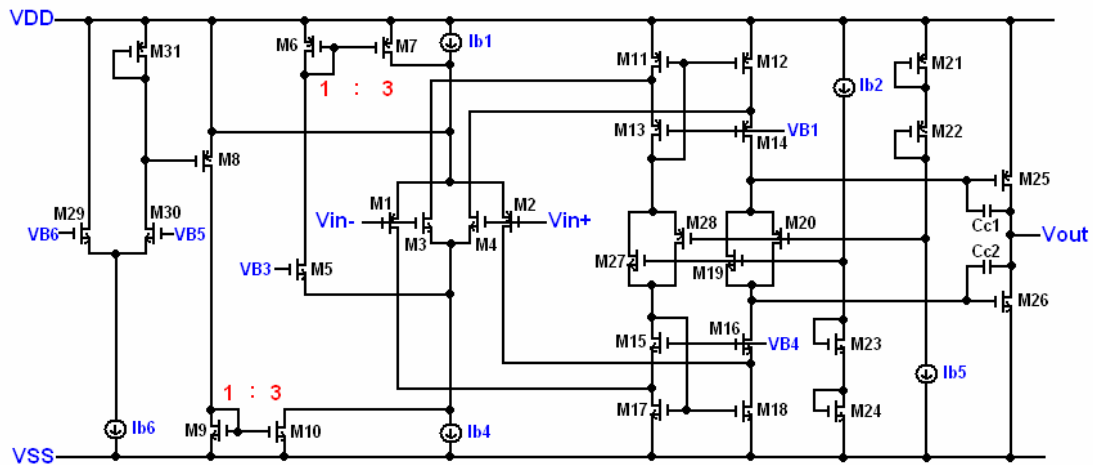

Fig 4.22 Hogervorst's class-AB amplifier [26]

In the intermediate part of the common-mode input range both current switches are off. The result is that the complementary input pairs are biased with a current of I_{ref}. And thus the tail currents obey Eq 4-20, in this part of the common-mode input

range. If the common-mode input voltage decreases below VB3, the current switch, M5, takes away the tail current of the N-channel input pair and feeds it into the current mirror M6-M7. Here it is multiplied by a factor three and added to the tail current of the P-channel input pair. The result is that the tail current of the P-channel input pair is equal to $4I_{ref}$. As a consequence, the tail currents again comply with Eq 4.13. From the above, it follows that the transconductance of the rail-to-rail input stage with g_m control by three-times current mirrors has the same value for each part of the common-mode input range. This transconductance is given by

$$g_m = \sqrt{2\mu C_{ox} \frac{W}{L} I_{ref}} \qquad (4\text{-}21)$$

At supply voltages below 2.9V both current switches might conduct at the same common-mode input voltage. To prevent this positive feedback loop, M5-M10, from becoming active, M29-M31 are added to the input stage. Each side of the differential pair, M29-M30, is connected via a voltage source, VB5 or VB6, to either one of the supply-rails. The differential pair measures the supply voltages. If the supply voltage is larger than a certain value, in this case 2.9V, the gate voltage of the current switch M8 is biased by M31. At supply voltages lower than 2.9V, the differential pair gradually turns off M31. Thus, the gate voltages of the P-channel current switch moves towards the positive supply rail, which means that it is always off at supply voltages below 2.9V. Hence, the positive feedback loop can never become active.

The floating class-AB control transistors, the stacked diode-connected transistors and the output transistors set up two translinear loops M20, M21, M22, M25 and M19, M23, M24, M26, which determine the quiescent current in the output transistors. The

class-AB action is performed by keeping the voltage between the gates of the output transistors constant. Suppose signal current sources are pushed into the class-AB output stage. As a result, the current of the P-channel class-AB transistor, M20, increases while the current in the N-channel class-AB transistors, M19, decreases by the same amount. Consequently, the gate-voltages of both the output transistors move up. Thus the output stage pulls a current from the output node.

The floating current source, M27-M28, has the same structure as the floating class-AB control. The value of the current source is set by two translinear loops, M11, M21, M22, M28 and M17, M23, M24, M27. The mirrors, M11-M14 and M15-M18, are loaded by the drain currents of the input pairs M1-M2 and M3-M4, respectively. These drain currents, and consequently the gate-source voltages of M11 and M17, change with the common-mode input voltage. If, for example, the common-mode input voltage approaches the positive supply rail, the g_m-control circuit increases the current of Ib1 and decreases the current of Ib2. As a result, the gate-source voltage of M11 decreases while the gate-source voltage of M17 increases. However, this hardly effects the value of the floating current source, M27-M28, because an increase of the gate-source voltage of one mirror compensates for a decrease in the other mirror. Since the floating current source, M27-M28, has the same structure as the class-AB driver circuit, M19-M20, the supply voltage dependency of the current mirror compensates for the supply voltage dependency of the class-AB driver. The result is a quiescent current which is insensitive to supply voltage variations.

4-4 Analog implementation of the Delta-Sigma Audio DAC

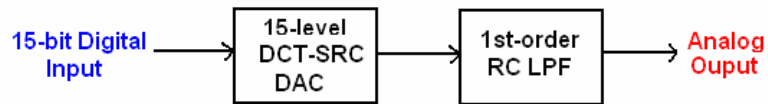Figure 4.23 shows the analog part circuit of 1.8V Delta-Sigma Audio DAC.

Fig 4.23 Analog part circuit of 1.8V delta-sigma DAC

An important feature to give robustness to the DR performance is the fact that the single-ended structure of the SC filter avoids the implementation of the CMFB. In a fully differential SC networks, the large output swing forces to use a common-mode feedback (CMFB) circuit implemented with SC technique, which may be a critical block in fully differential structure since it requires to re-charge at any clock cycle fully discharged capacitors. This causes spikes and sometimes, slew rate which increases total harmonic distortion(THD). Combine the direct charge transfer (DCT) technique, and switched-RC techniques. The proposed DCT-SRC DAC circuit is shown in Fig4.24.
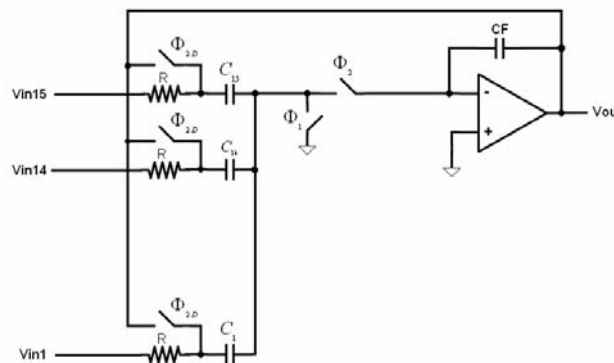

Fig 4.24 Proposed DCT-SRC DAC

The amplifier which is used in DCT-SRC DAC is a folded cascode op amp. The schematic of this amplifier is shown in Fig 4.25 and spec of the amplifier is listed in Table 4.2.
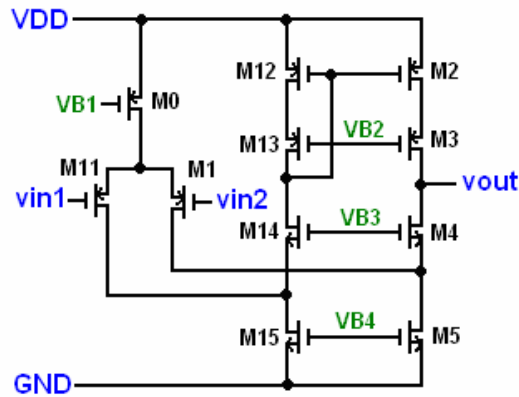
Fig 4.25 Folded cascode op amp

	SS	TT	FF
DC Gain	57dB	57dB	55dB
Phase Margin	67.5^o	67°	66.8^o
Unit gain bandwidth	508MHz	539MHz	567MHz
Supply voltage	1.8V	1.8V	1.8V

Table 4.2 Spec of folded cascode op amp

A 1st-order LPF shown in Fig 4.26 is used to filter out-of-band noise. The pole frequency is sloppily defined due to RC variation. However, in audio application, the cut-off frequency can be around 10 times higher than the audio bandwidth. Hence the variation of pole frequency will not affect the frequency response of the band-of-interest. The quality factor of Q=0.707, and -3dB cut-off frequency fc=150kHz.

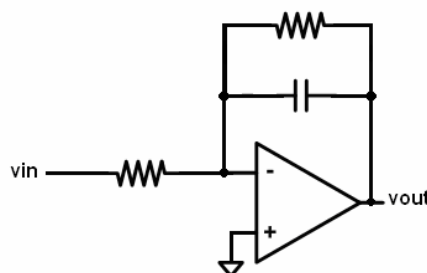**Fig 4.26 1st order RC low pass filter**

Figure 4.27 shows the schematic of the designed Class AB amplifier, which is used in low pass filter. Crossover distortion is controlled by making M9 and M10 not turn off completely in the quiescent condition. Table 4.3 shows the spec of the class AB amplifier.
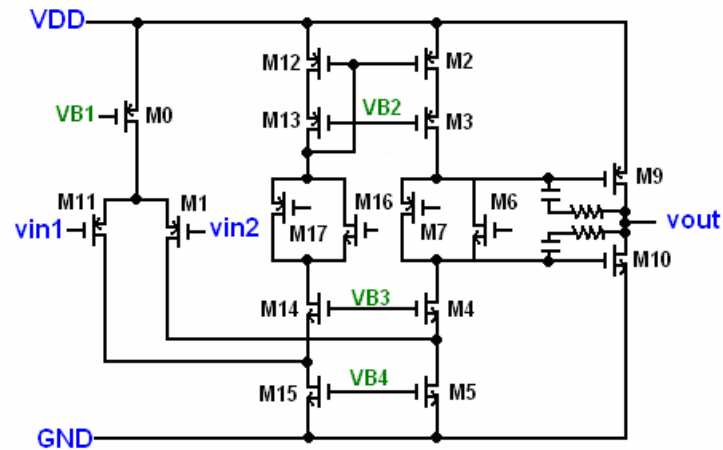

Fig 4.27 Class AB amplifier

	SS	TT	FF
DC Gain	101dB	105dB	100dB
Phase Margin	61	62.3	65
Unit gain bandwidth	285MHz	291MHz	305MHz
Supply voltage	1.8V	1.8V	1.8V

Table 4.3 Spec of Class AB opamp

The chip layout of the designed DAC is show in Fig 4.28. It was fabricated in TSMC $0.18\mu m$ 1P6M process. The core area is about $0.526mm^2$. The chip is packaged in 68-pin LCC.

The SNDR at -6dBFS is 70dB, which is mainly dominated by the distortion. This can by seen in Fig.4.29, which shows the output spectrum for a -6dBFS input signal amplitude at 1kHz. For audio applications, the DR is usually calculated as SNDR at -60dBFS (whose spectrum is shown in Fig.4.28), which is 31dB. This yields a 91dB dynamic range. Fig.4.30 shows the out-of-band noise spectrum. Fig.4.31 shows the SNDR versus input level form -85 to 0dBFS for a 1kHz input signal.

The DAC performance summary is presented in Table4.4.
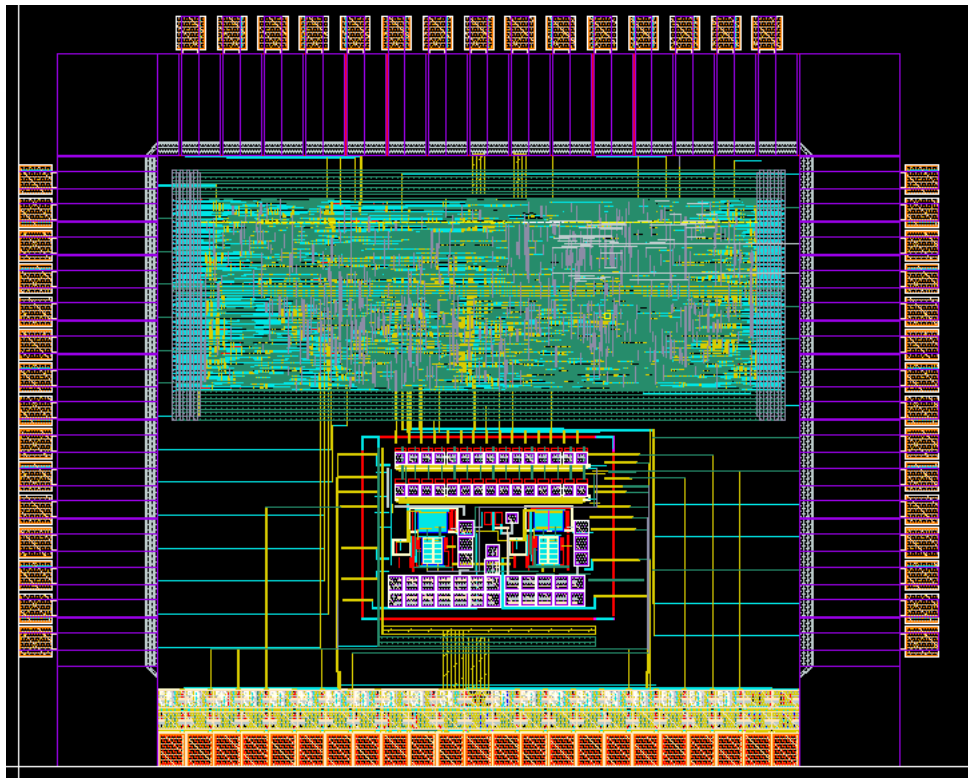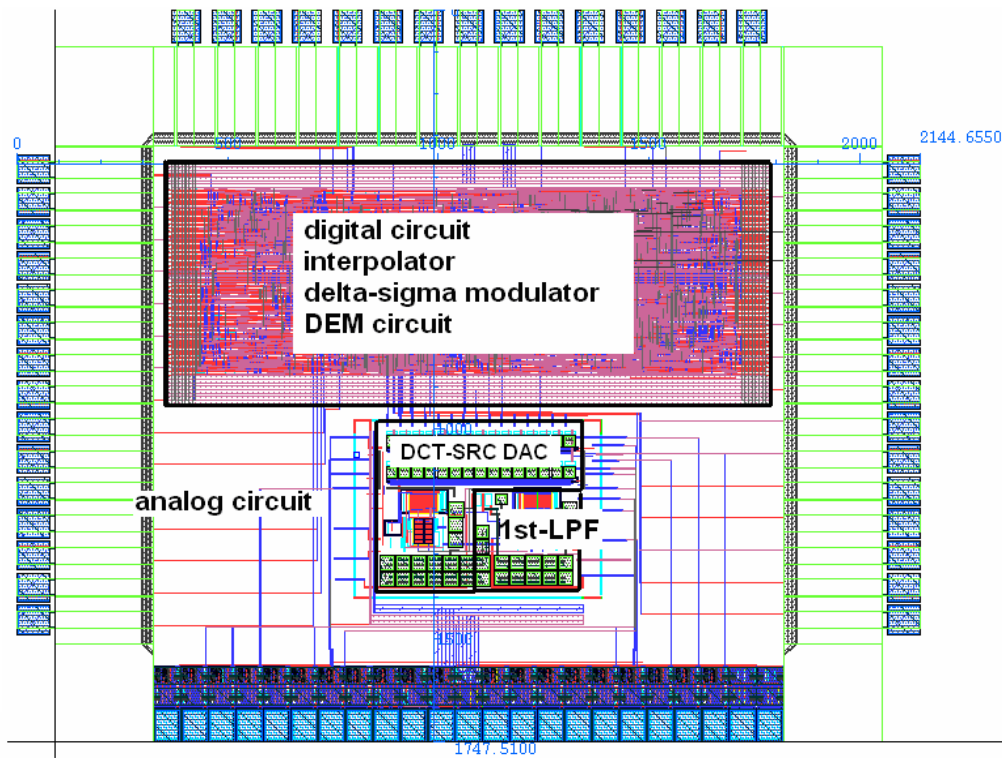
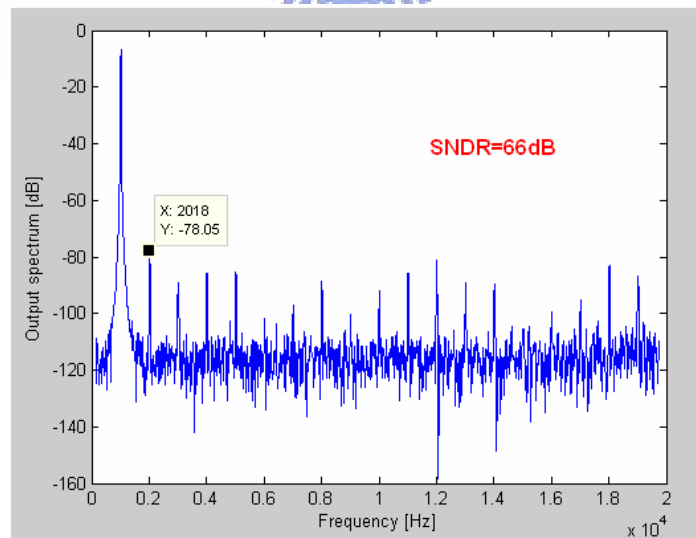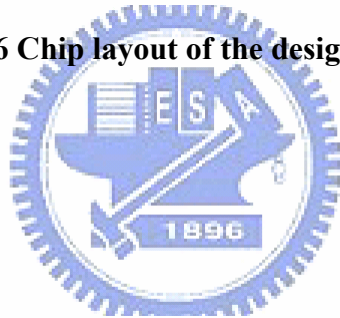**Fig 4.26 Chip layout of the designed DAC**

Fig 4.27 Output spectrum of a 1kHz input signal with –6dBFS
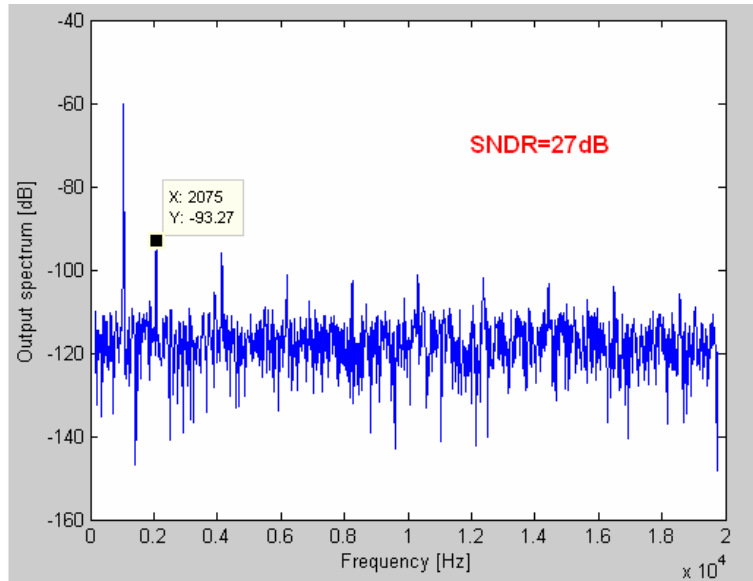
Fig 4.28 Output spectrum of a 1kHz input signal with -60dBFS
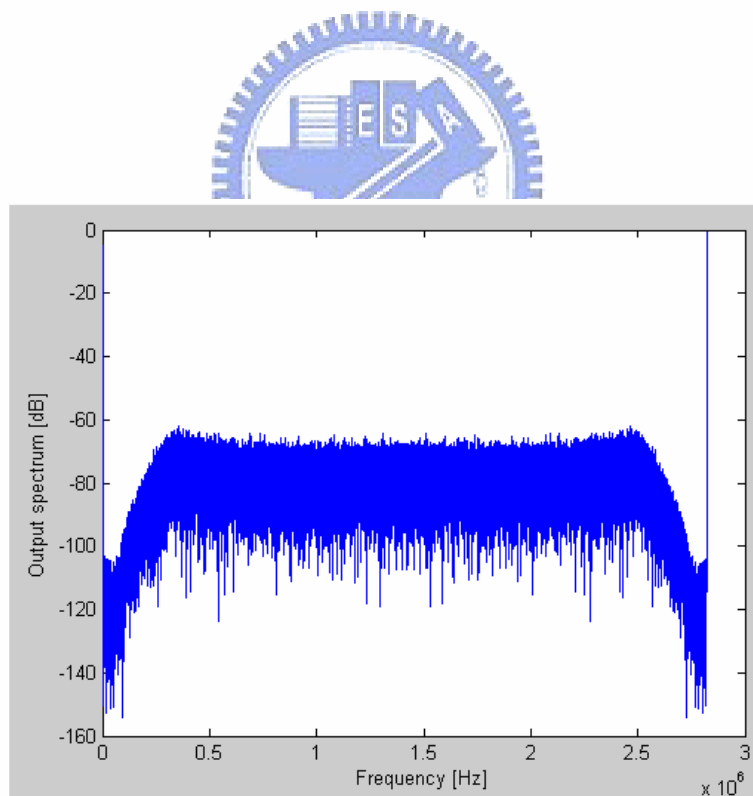
Fig 4.29 Output-of-band noise spectrum
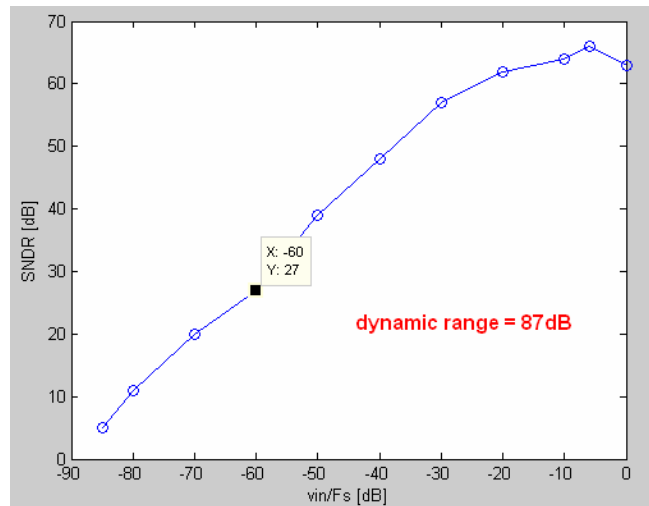
Fig 4.30 Simulation SNDR

Parameter	Value
Power supply	Digital=1.8V Analog=1.8V
Signal Bandwidth	20kHz
Sampling frequency	2.8224MHz
Oversampling ratio	64
Power consumption	Digital=0.25mW Analog=8mW
Output range	0.8Vpp
Peak SNDR	66dB@-6dBFS
Dynamic range	87dB
Technology	TSMC $0.18\mu m$ CMOS
Active die area	Digital=$0.34mm^2$ Analog=$0.186mm^2$
Chip area (including pad)	$3.756mm^2$

Table 4.3 The performance of the designed DAC (post-simulation)

Chapter 5

Conclusions

5.1 Summary

Oversampling delta-sigma techniques used in the audio DACs were discrbied in this thesis. The associated topics have also been studied in detail.

These include:

A digital interpolator and noise shaper have been designed and analyzed. A thermometer encoder and a data weighted averaging encoder is implemented.

Different architectures of internal DAC and different types of class AB amplifier are discussed.

An audio DAC using DCT-SRC technique was built, and simulation showed it approach a typical high-end audio requirement.

5.2 Future Work

Improve SNDR and try to design internal DAC with VDD smaller than 1V.

Bibliography

[1]   P. Ju, K. Suyama, P. F. Ferguson, Jr., and W. Lee, "A 22-kHz Multibit Switched-Capacitor Sigma-Delta D/A Converter with 92 dB Dynamic Range", IEEE Journal of Solid-State Circuits, vol. 30, no. 12, Dec. 1995.

[2]   P. Kiss, J. Arias, D. Li, and V. Boccuzzi, "Stable High-Order Delta–Sigma Digital-to-Analog Converters", IEEE Transactions on Circuits and Systems—I: Regular Papers, vol. 51, no. 1, January 2004

[3]   D.A. Johns and K. Martin, "Analog Integrated Circuit Design", John Wiley & Sons, Inc., 1997.

[4]   S.K.Mitra, Digital signal processing – a computer based approach, second edition, McGraw-Hill Companies, Inc., 2001

[5]   K. K. Parhi, VLSI Digital Signal Processing Systems: Design and Implementation. John Wiley & Sons, 1999

[6]   R. Schreier, and G.C.Temes, Understanding Delta-Sigma Data Converters, IEEE Press, 2005.

[7]   王勝賢，"應用於音頻數位/類比轉換器之多位元三角積分調變系統設計與實現"，國立台灣大學/電信工程學研究所/95/碩士/ 094NTU05435049

[8]   Delta-Sigma toolbox (http://www.math-works.com/matlabcentral/fileexchange)

[9]   L. R. Carley, "A noise-shaping coder topology for 15+ bit converters," IEEE Journal of Solid-State Circuits, vol. 24, pp. 267–273, Apr. 1989.

[10]   R. Schreier and B. Zhang, "Noise shaped multibit D/A converter employing unit elements," Electron. Lett., vol. 31, no. 20, pp. 1712–1713, Sept. 1995.

[11]   R. T. Baird and T. S. Fiez," Linearity Enhancement of Multibit AY, A/D and D/A Converters Using Data Weighted Averaging", IEEE Transactions on Circuits and Systems -I1 Analog and Digital Signal Processing, vol. 42, no. 12, Dec. 1995.

[12]   V. Colonna, M. Annovazzi, G. Boarin, G. Gandolfi, F. Stefani, and A. Baschirotto, "A 0.22-mm^2 7.25-mW per-Channel Audio Stereo-DAC With 97-dB DR and 39-dB SNR$_{out}$", IEEE Journal of Solid-State Circuits, vol. 40, no. 7, July 2005.

[13]   Fujimori, United States Patent 5990819

[14]   I. Fujimori and T. Sugimoto, "A 1.5 V, 4.1 mW Dual-Channel Audio Delta–Sigma D/A Converter", IEEE Journal of Solid-State Circuits, vol. 33, no. 12, Dec. 1998.

[15]   I. Fujimori, A. Nogi, and T. Sugimoto, "A Multibit Delta–Sigma Audio DAC

with 120-dB Dynamic Range", IEEE Journal of Solid-State Circuits, vol. 35, no. 8, August 2000.

[16] M. Annovazzi, V. Colonna, G. Gandolfi, F. Stefani, and A. Baschirotto, "A Low-Power 98-dB Multibit Audio DAC in a Standard 3.3-V 0.35-μm CMOS Technology", IEEE Journal of Solid-State Circuits, vol. 37, no. 7, July 2002

[17] Ruopeng Wang, Sang-Ho Kim, Sang-Hyeon Lee, Seung-Bin You, Jae-Whui Kim, Un-Ku Moon, Gabor, C. Temes, "A 100dB gain-corrected delta-sigma audio DAC with headphone driver", Analog Integr Circ Sig Process 2007

[18] Q.Meng, K.Lee, T.Sugimoto, K. Hamashita, K. Takasuka, S.Takeuchi, U.Moon, G.C. Temes, "A 0.8V, 88dB dual-channel audio ΔΣDAC with headphone driver," Symposium on VLSI Circuits, pp. 53-54, Jun. 2006.

[19] Y. Nakagome et al., "A 1.5V circuit technology for 64mb drams," in IEEE International Symposium on VLSI Circuits, Digest of Technical Papers, Jun. 1990, pp. 17-18.

[20] J. Steensgaard, "Bootstrapped low-voltage analog switches," Proceedings of the 1999 IEEE International Symposium on Circuits and Systems, Volume 2, pp.29- 32, May 30 – June 2, 1999.

[21] G.Ahn, D. Chang, M. Brown, N. Ozaki, H.Youra, K. Yamamura, K. Hamashita, K. Takasuka, G. C. Temes, and U. Moon, "A 0.6-V 82dB delta-sigma audio ADC using switched-RC integrators," IEEE J.Solid-State Circuits, vol.40, no.12, pp. 2398-2407, Dec. 2005.

[22] R. Castello, P.Gray, "A high-performance micropower switched-capacitor filter", IEEE Journal Solid-State Circuits, Vol SC 20, pp.1122-1132, Dec.1985.

[23] J. Fischer, R. Koch, "A highly linear CMOS buffer amplifier", IEEE Journal Solid State Circuits, Vol. SC 22, pp 330-334, June 1987.

[24] M.Degrauwe, J. Rijmenants, E. A. Vittoz, "Adaptive Biasing CMOS Amplifiers", IEEE Journal of Solid State Circuits, Vol. SC 17, No. 3, June 1982.

[25] Wen-Chung S. Wu, Ward J. Helms, Jay A. Kuhn, and Bruce E. Byrkett, "Digital-Compatible High-Performance Operational Amplifier with Rail-to-Rail Input and Output Ranges", IEEE Journal of Solid State Circuits, Vol. 29, No.1, January 1994.

[26] R. Hogervorst, John P. Tero, Ruud G. H. Eschauzier, and Johan H. Huijsing, "A Compact Power-Efficient 3V CMOS Rail-to-Rail Input/Output Operational Amplifier for VLSI Cell Libraries", IEEE Journal of Solid State Circuits. Vol. 29. No.12. December 1994.